Multipion and Strange-Particle Photoproduction on Protons at Energies up to 5.8 GeV

AACHEN–BERLIN–BONN–HAMBURG–HEIDELBERG–MÜNCHEN COLLABORATION

R. ERBE, H. G. HILPERT, E. SCHÜTTLER, AND W. STRUCZINSKI
III. Physikalisches Institut der Technischen Hochschule, Aachen, Germany

AND

K. LANIUS, A. MEYER, A. POSE, AND H. J. SCHREIBER
Institut für Hochenergiephysik, Deutsche Akademie der Wissenschaften zu Berlin, Berlin-Zeuthen, Germany

AND

W. JOHNSSEN, J. MOEBES*, B. NELLEN, AND W. TEJESSY*
Physikalisches Institut der Universität Bonn und KFA Jülich, Bonn, Germany

AND

G. HORLITZ, E. LOHRMANN, H. MEYER, W. P. SWANSON†, M. W. TEUCHER, G. WOLF†, AND S. WOLFF
Deutsches Elektronen-Synchrotron DESY, Hamburg, Germany

AND

H. ALVENSLEBEN, D. LÜKE, H. SPITZER, AND F. STORIM
Physikalisches Staatsinstitut, II. Institut für Experimentalphysik Hamburg, Germany

AND

H. BEISEL, H. FILTHUTH, H. KOLAR, AND P. STEFFEN
Institut für Hochenergiephysik der Universität Heidelberg, Heidelberg, Germany

AND

P. FREUND, K. GOTTSTEIN, N. SCHMITZ, P. SEYBOTH†, AND J. SEYERLEIN
Max-Planck-Institut für Physik und Astrophysik, München, Germany

(Received 18 July 1969)

In a study of photoproduction at photon energies between 0.3 and 5.8 GeV in a hydrogen bubble chamber, approximately 1.7 million pictures containing about 31 000 events with three or more outgoing charged particles were analyzed. This is the second of two final reports on this experiment. Distributions of effective masses are given for the reactions $\gamma p \to N3\pi$, $N4\pi$, $N5\pi$. Cross sections for the production of $\Delta(1236)$ and ρ via $\gamma p \to \Delta\rho$, $\Delta 2\pi$, $\Delta 3\pi$, $\Delta 4\pi$, $N\pi\rho$, and $N2\pi\rho$ and of various other reactions are reported. From the reaction $\gamma p \to \Delta^{++}\rho^-$, an upper limit for the radiative decay width of ρ^-, $\Gamma(\rho^- \to \pi^-\gamma) < 0.24$ MeV, is obtained (90% confidence). For the four-pion decay mode of the ρ^0, an upper limit of $\Gamma(\rho^0 \to \pi^+\pi^+\pi^-\pi^-)/\Gamma(\rho^0 \to \pi^+\pi^-) < 0.0015$ is found (90% confidence). The photoproduction of strange particles is discussed and cross sections for $\gamma p \to \Lambda K^+$, ΣK, $\Lambda K\pi$, $\Sigma K\pi$, and $\Lambda K\pi\pi$ are presented. Production of $\Sigma(1385)$ was observed.

I. INTRODUCTION

THIS is the second of two final reports on a bubble-chamber experiment to study photoproduction of hadrons at energies up to 5.8 GeV. The experiment was carried out in the 85-cm hydrogen bubble chamber at DESY exposed to an approximate bremsstrahlung beam. In the first report, the experimental procedure was described, and total cross sections for final states not involving strange particles were given.[1] The production cross sections and decay distributions for the reactions $\gamma p \to pV$, $(V=\rho^0, \omega, \phi)$ $\gamma p \to \Delta\pi$, $[\Delta=\Delta^{++}(1236), \Delta^0(1236)]$, $\gamma p \to p\eta$, and $\gamma p \to pX^0$ were also discussed in Ref. 1. In the present paper (Secs. III and IV), the production of the resonances Δ and ρ in the reactions

$$\gamma p \to p\pi^+\pi^-\pi^0, \tag{1}$$

$$\gamma p \to n\pi^+\pi^+\pi^- \tag{2}$$

is studied. From analysis of the reaction $\gamma p \to \Delta^{++}\rho^-$, an upper limit for the radiative decay width of the ρ^- meson, $\Gamma(\rho^- \to \pi^-\gamma)$, is obtained. In Sec. V, we report on the production of the resonances Δ, ρ, ω, ϕ, η in the reactions

$$\gamma p \to p\pi^+\pi^+\pi^-\pi^-, \tag{3}$$

$$\gamma p \to p\pi^+\pi^+\pi^-\pi^-\pi^0, \tag{4}$$

$$\gamma p \to n\pi^+\pi^+\pi^+\pi^-\pi^-, \tag{5}$$

$$\gamma p \to p\pi^+\pi^-K^+K^-, \tag{6}$$

$$\gamma p \to p\pi^+\pi^-K^0\bar{K}^0. \tag{7}$$

* Present address: CERN, Geneva, Switzerland.
† Present address: SLAC, Stanford, Calif.
[1] Aachen-Berlin-Bonn-Hamburg-Heidelberg-München Collaboration, Phys. Rev. **175**, 1669 (1968).

TABLE I. Number of events found for various reactions. (A) Number of events found in two scans. (B) Number of events corrected for scanning losses. The number of 3- and 5-prong events given in the Table correspond to a flux of 9.1×10^7 equivalent quanta with $E_\gamma>0.1$ GeV. The 7-prong events correspond to 8.6×10^7 equivalent quanta. The scanning volume used had a length of 45 cm.

Hypothesis considered by GRIND	Number of constraints	Number of events (A) found	(B) corrected
(1) $\gamma p \to p\pi^+\pi^-$	3	18 780	19 020
(2) $\gamma p \to p\pi^+\pi^-\pi^0$[a]	0	6 770	6 800
(3) $\gamma p \to n\pi^+\pi^+\pi^-$[a]	0	3 020	3 050
Ambiguous between (2) and (3)[a]	0	1 310	1 330
(4) $\gamma p \to p\pi^+\pi^+\pi^-\pi^-$	3	590	590
(5) $\gamma p \to p\pi^+\pi^+\pi^-\pi^-\pi^0$[a]	0	600	600
(6) $\gamma p \to n\pi^+\pi^+\pi^+\pi^-\pi^-$[a]	0	250	250
Ambiguous between (5) and (6)[a]	0	200	200
(7) $\gamma p \to p3\pi^+3\pi^-$	3	18	18
(8) $\gamma p \to p3\pi^+3\pi^-\pi^0$[a]	0	16	16
(9) $\gamma p \to n4\pi^+3\pi^-$[a]	0	7	7
Strange-particle hypotheses (see Table VI)		1 312	
Unassigned events:			
3-prong events	No fit with proton		427
	No fit without proton		16
	Unmeasurable		510
5-prong events	No fit		18
	Unmeasurable		89
7-prong events	No fit		1
	Unmeasurable		10

[a] The events from these reactions are contaminated by events with two or more unobserved outgoing neutral particles.

Section VII gives an account of strange-particle production.

Preliminary results, based on part of the statistics, have already been published in Refs. 2 and 3. Some results from the final statistics that were reported in Refs. 4 and 5 are included here for completeness. An experiment, similar to the one described here, was carried out at CEA by the Cambridge Bubble-Chamber Group. Their results on strange-particle production and multipion production have been reported in Refs. 6 and 7. The results of the two experiments are in reasonable agreement, except for a discrepancy in the cross section of the reaction $\gamma p \to \Delta^{++}\rho^-$, which is discussed in Sec. III C.

II. KINEMATIC ANALYSIS

The kinematic analysis was done using the CERN program GRIND as described in Ref. 1. Because the photon energy was unknown, events with more than one outgoing neutral particle (multineutral events) could not be analyzed correctly. They were analyzed in GRIND as if only one neutral particle had been produced. Multineutral events with an outgoing proton were analyzed by GRIND as if a single π^0 had been produced, whereas multineutral events with an outgoing neutron were analyzed as if the neutron was the only neutral particle produced.

Table I gives the number of events found for various reactions; it also contains the number of events corrected for scanning losses. Events labeled as ambiguous in Table I could not be assigned to a particular reaction. When analyzing a reaction, the unique events were examined together with the ambiguous ones, so that no event of the reaction was lost.

When studying resonance production in final states involving neutral particles, two cases can be distinguished:

(1) The final state contains only *one* neutral particle (e.g., $\gamma p \to p\pi^+\pi^-\pi^0$). Then the kinematics are uniquely determined. The calculated photon energy is correct within the measurement errors. Any produced resonance can be observed in the corresponding invariant mass spectrum, e.g., $\gamma p \to \Delta^{++}\rho^- \to (p\pi^+)(\pi^-\pi^0)$.

(2) The final state contains *two* or *more* neutral particles (e.g., $\gamma p \to p\pi^+\pi^-\pi^0\pi^0$, analyzed as $\gamma p \to p\pi^+\pi^-\pi^0$). Then the photon energy computed by GRIND is systematically too low because of the misinterpretation of the neutral particles. Considering resonance production in multineutral final states, two cases must be distinguished:

(a) If a resonance is produced which decays into charged particles only, its invariant mass spectrum is not influenced by the kinematic analysis, e.g., $\gamma p \to \Delta^{++}\pi^-\pi^0\pi^0 \to (p\pi^+)\pi^-\pi^0\pi^0$ analyzed as $\gamma p \to p\pi^+\pi^-\pi^0$.

[2] Aachen-Berlin-Bonn-Hamburg-Heidelberg-München Collaboration, Nuovo Cimento **48A**, 262 (1967); multipion production.

[3] Aachen-Berlin-Bonn-Hamburg-Heidelberg-München Collaboration, Nuovo Cimento **49A**, 504 (1967); **51A**, 246 (1967); strange-particle production.

[4] Aachen-Berlin-Bonn-Hamburg-Heidelberg-München Collaboration, Phys. Letters, **27B**, 54 (1968); vector-meson production.

[5] E. Lohrmann, in *Proceedings of the 1967 International Symposium on Electron and Photon Interactions at High Energies, Stanford Linear Accelerator Center, 1967* (Clearinghouse for Federal Scientific and Technical Information, National Bureau of Standards, U. S. Department of Commerce, Springfield, Va., 1968), p. 199.

[6] Cambridge Bubble-Chamber Group, Phys. Rev. **156**, 1426 (1967); strange-particle production.

[7] Cambridge Bubble-Chamber Group, Phys. Rev. **169**, 1081 (1968); multipion production.

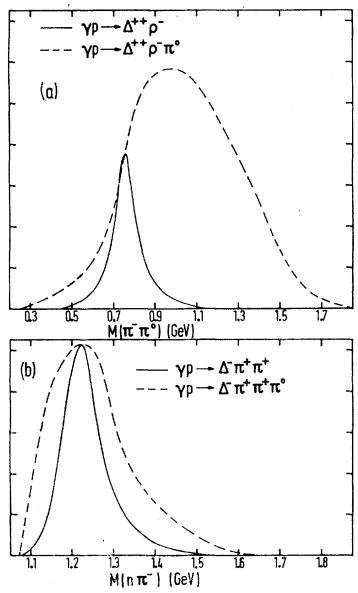

FIG. 1. Mass distributions generated by a Monte Carlo program. (a) $\pi^-\pi^0$ mass distribution for $3.5<E_\gamma<5.8$ GeV. The full curve shows the resonance shape of a ρ^- produced in $\gamma p \to \Delta^{++}\rho^-$; the dashed curve shows $M(\pi^-\pi^0)$ for events from reaction $\gamma p \to \Delta^{++}\rho^-\pi^0 \to p\pi^+\pi^-\pi^0\pi^0$ when analyzed as $\gamma p \to p\pi^+\pi^-\pi^0$. E_γ is the photon energy obtained from this analysis. (b) $n\pi^-$ mass distribution for $1.4<E_\gamma<1.8$ GeV. The full curve shows the resonance shape for a Δ^- produced in $\gamma p \to \Delta^-\pi^+\pi^+$; the dashed curve shows $M(n\pi^-)$ for events from reaction $\gamma p \to \Delta^-\pi^+\pi^+\pi^0 \to n\pi^-\pi^+\pi^+\pi^0$ when analyzed as if the reaction were $\gamma p \to n\pi^-\pi^+\pi^+$. The dashed curve is scaled so that it cuts the maximum of the full curve.

(b) If among the decay products of the resonance there is one neutral particle, then the mass of the resonance cannot be measured correctly, and the resonance peak will, in general, not be found. For instance,

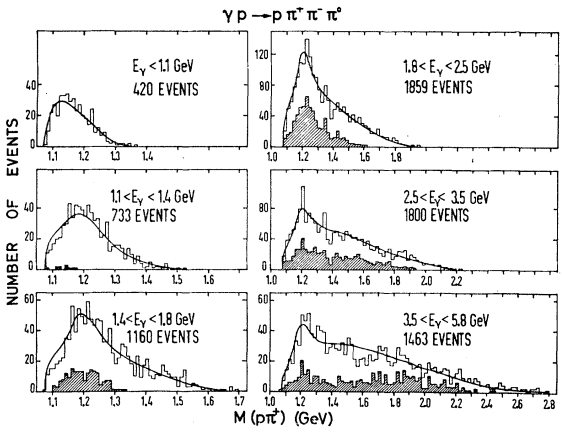

FIG. 2. Reaction $\gamma p \to p\pi^+\pi^-\pi^0$. Distributions of the $p\pi^+$ effective mass $M(p\pi^+)$, for six intervals of the photon energy. The events ambiguous between reactions $\gamma p \to p\pi^+\pi^-\pi^0$ and $\gamma p \to n\pi^+\pi^+\pi^-$ are included in Figs. 2–7. The curves are the sum of contributions from Lorentz-invariant phase space, from the processes $\gamma p \to p\eta$ and $\gamma p \to p\omega$ and from all resonance-production processes listed in Table II for the respective photon-energy intervals. The shaded areas give the distributions of events with $0.63<M(\pi^-\pi^0)<0.89$ GeV.

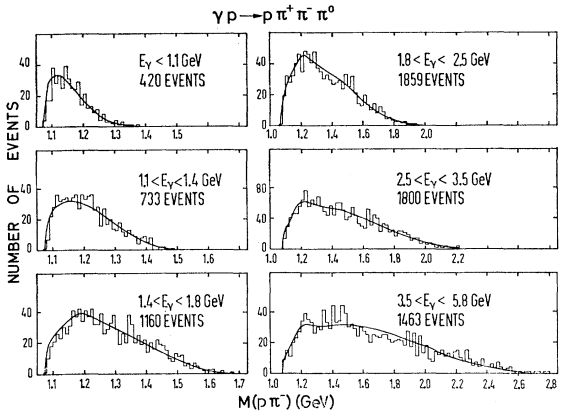

FIG. 3. Reaction $\gamma p \to p\pi^+\pi^-\pi^0$. Distributions of the $p\pi^-$ effective mass $M(p\pi^-)$. The curves have the same meaning as in Fig. 2.

the reaction $\gamma p \to p\pi^+\rho^-\pi_2{}^0 \to p\pi^+(\pi^-\pi_1{}^0)\pi_2{}^0$ is analyzed as $\gamma p \to p\pi^+\pi^-\pi^0$, with a fictitious π^0 substituted for the neutral $\pi_1{}^0\pi_2{}^0$ system in the kinematic analysis. The invariant mass $M(\pi^-\pi^0)$ thus obtained will have a spectrum much broader than the original resonance shape. This effect can be seen in Fig. 1(a). The dashed curve shows the distribution of the invariant mass $M(\pi^-\pi^0)$ for Monte Carlo events of the reaction $\gamma p \to \Delta^{++}\rho^-\pi_2{}^0 \to (p\pi^+)(\pi^-\pi_1{}^0)\pi_2{}^0$ analyzed as $\gamma p \to p\pi^+\pi^-\pi^0$, with a calculated photon energy between 3.5 and 5.8 GeV. The mass distribution $M(\pi^-\pi^0)$ one obtains is quite different from the resonance shape $M(\pi^-\pi_1{}^0)$ of the ρ^-, which is also shown in Fig. 1(a) (full curve). Therefore, events of the reaction $\gamma p \to \Delta^{++}\rho^-\pi^0$ hardly contaminate the cross section for reaction $\gamma p \to \Delta^{++}\rho^-$ (for photon energy 3.5–5.8 GeV), which is determined from the analysis of the invariant mass distributions.

On the other hand, when events of the reaction $\gamma p \to \Delta^-\pi^+\pi^+\pi^0 \to (n\pi^-)\pi^+\pi^+\pi^0$ are analyzed as $\gamma p \to$

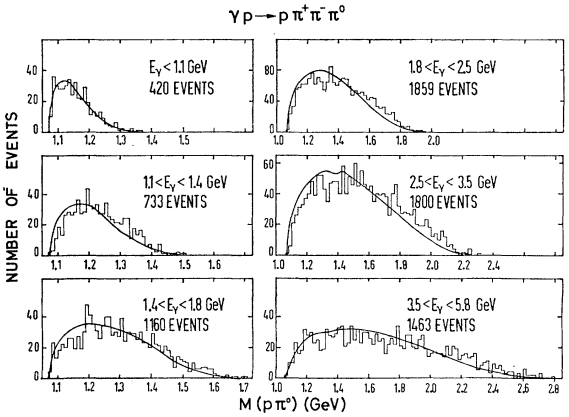

FIG. 4. Reaction $\gamma p \to p\pi^+\pi^-\pi^0$. Distributions of the $p\pi^0$ effective mass $M(p\pi^0)$. The curves have the same meaning as in Fig. 2.

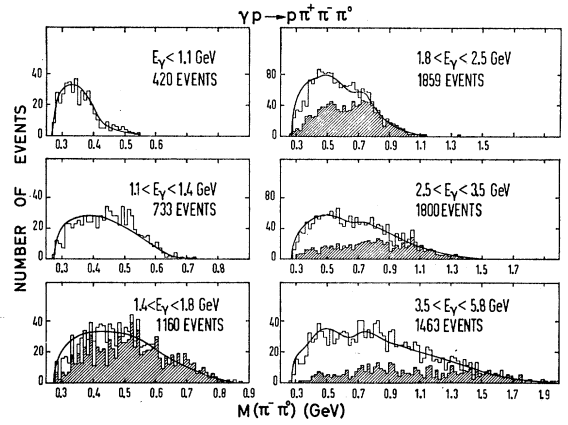

FIG. 5. Reaction $\gamma p \to p\pi^+\pi^-\pi^0$. Distributions of the $\pi^-\pi^0$ effective mass $M(\pi^-\pi^0)$. The curves have the same meaning as in Fig. 2. The shaded areas give the distributions of events with $1.10 < M(p\pi^+) < 1.34$ GeV.

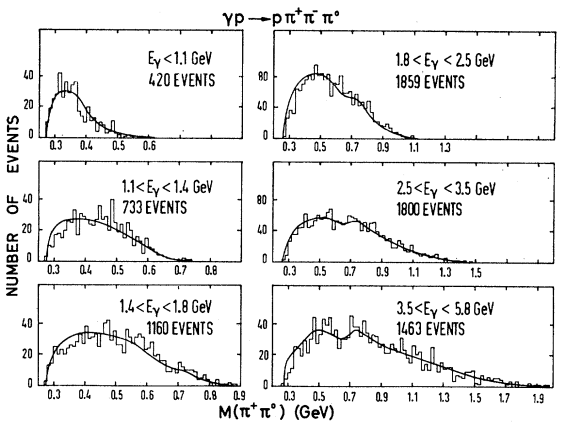

FIG. 6. Reaction $\gamma p \to p\pi^+\pi^-\pi^0$. Distributions of the $\pi^+\pi^0$ effective mass $M(\pi^+\pi^0)$. The curves have the same meaning as in Fig. 2.

$n\pi^-\pi^+\pi^+$, the invariant mass $M(n\pi^-)$ so obtained does not differ very much from the Δ^--resonance shape. This is shown, using Monte Carlo events, in Fig. 1(b) for calculated photon energy within 1.4 and 1.8 GeV. Therefore, cross sections determined for $\gamma p \to \Delta^-\pi^+\pi^+$ (for photon energy 1.4–1.8 GeV) may be contaminated by the reaction $\gamma p \to \Delta^-\pi^+\pi^+\pi^0$. In the following sections, we will make use of these and similar Monte Carlo results that we obtained.

III. REACTION $\gamma p \to p\pi^+\pi^-\pi^0$

A. Cross Sections

The procedure to calculate cross sections has been described in Ref. 1. Since the reaction

$$\gamma p \to p\pi^+\pi^-\pi^0 \tag{1}$$

is contaminated by events with two or more π^0 and by ambiguous events which really may belong to reaction $\gamma p \to n\pi^+\pi^+\pi^-$, only upper limits could be determined for the cross section of reaction (1). They were given in Ref. 1. From experiments with known photon energy, cross sections of about 20 μb have been obtained for photon energies between 3 and 5 GeV.[8,9]

The cross sections for the reactions $\gamma p \to p\pi^+\pi^-\pi^0\pi^0$ and $\gamma p \to p\pi^+\pi^-\pi^0\pi^0\pi^0$ may be estimated with the method of Satz.[10,11] This makes use of vector dominance, the additive quark model, an isospin-independence assumption, and experimental πp cross sections to predict cross sections for multipion photoproduction on protons. The predictions of Satz agree reasonably well with measured photoproduction cross sections.[1,8–10] For multineutral reactions we get from this model the predictions

$$\sigma(\gamma p \to p\pi^+\pi^-\pi^0\pi^0)/\sigma(\gamma p \to p\pi^+\pi^+\pi^-\pi^-) = 1.63,$$

$$\sigma(\gamma p \to p\pi^+\pi^-\pi^0\pi^0\pi^0)/\sigma(\pi^+ p \to p\pi^+\pi^+\pi^+\pi^-\pi^-) = 0.00433.$$

Using in the denominator the cross sections obtained in this experiment and in Ref. 12, one calculates, e.g., at $E_\gamma = 4$ GeV,

$$\sigma(\gamma p \to p\pi^+\pi^-\pi^0\pi^0) = 9 \pm 1\ \mu\text{b},$$

$$\sigma(\gamma p \to p\pi^+\pi^-\pi^0\pi^0\pi^0) = 1.1 \pm 0.2\ \mu\text{b}.$$

B. Mass Distributions and Fitting Procedure

Figures 2–7 show the two-particle mass distributions of reaction (1) for six photon-energy intervals. The events which are ambiguous between reactions (1) and

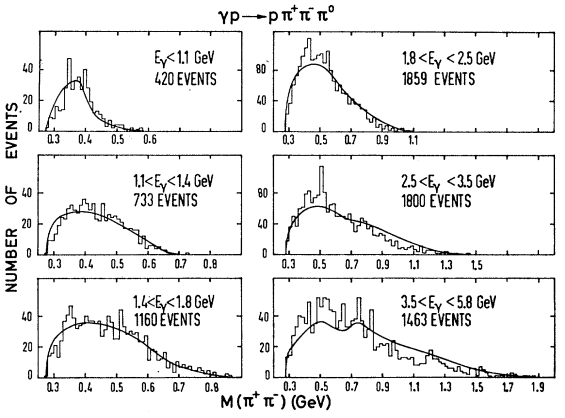

FIG. 7. Reaction $\gamma p \to p\pi^+\pi^-\pi^0$. Distributions of the $\pi^+\pi^-$ effective mass $M(\pi^+\pi^-)$. The curves have the same meaning as in Fig. 2.

[8] J. Ballam *et al.*, Phys. Rev. Letters **21**, 1541 (1968); Y. Eisenberg *et al.*, *ibid.* **22**, 669 (1969).

[9] H. Baisch, Diplomarbeit, Hamburg, 1968 (unpublished).

[10] H. Satz, Phys. Letters **25B**, 27 (1967); and (private communications).

[11] H. Satz, Phys. Rev. Letters **19**, 1453 (1967).

[12] Aachen-Berlin-Birmingham-Bonn-Hamburg-London (I.C.)-München Collaboration, Phys. Rev. **138**, B897 (1965); Aachen-Berlin-Bonn-Hamburg-München Collaboration, Nuovo Cimento **44**, 530 (1966).

TABLE II. Reaction $\gamma p \to p\pi^+\pi^-\pi^0$. Cross sections ($\mu$b) for various resonance-production processes. The columns labeled UL give upper limits for the cross sections because of contamination by multineutral events.

E_γ (GeV)	$\Delta^{++}\rho^-$	$\Delta^+\rho^0$	$\Delta^0\rho^+$	UL $\Delta^{++}\pi^-\pi^0$	UL $\Delta^+\pi^+\pi^-$	UL $\Delta^0\pi^+\pi^0$	$p\pi^+\rho^-$	UL $p\pi^0\rho^0$	$p\pi^-\rho^+$
1.1–1.4	···	···	···	4.0±0.8	1.8±0.8	···	···	···	···
1.4–1.8	1.4±0.6	···	1.2±0.9	6.7±1.2	···	···	···	···	···
1.8–2.5	2.1±0.9	···	0.6±0.8	6.4±1.2	···	1.4±1.1	1.5±1.0	···	2.1±1.0
2.5–3.5	1.5±0.6	···	0.1±0.6	5.7±1.0	···	3.2±0.8	0.1±0.8	···	2.6±0.9
3.5–5.8	0.8±0.3	0.5±0.3	0.6±0.3	2.7±0.6	···	0.8±0.5	0.8±0.6	1.4±0.5	1.4±0.6

(2) have been included. Figure 2 gives evidence for the production of the isobar $\Delta^{++}(1236)$. Indications for production of the resonances Δ^0, ρ^-, and ρ^+ are very weak (Figs. 3, 5, and 6). In the $\pi^+\pi^-\pi^0$ mass distribution (see Ref. 1), the production of ω and η mesons is observed; this was discussed in Ref. 1. The other three-particle mass distributions do not show any obvious resonance production.

A sum of noninterfering contributions of the following processes was fitted to the observed density distribution of the effective masses, using a maximum likelihood method:

(a) double-resonance production,

$$\gamma p \to \Delta^{++}\rho^-, \quad \gamma p \to \Delta^+\rho^0, \quad \gamma p \to \Delta^0\rho^+;$$

(b) isobar production,

$$\gamma p \to \Delta^{++}\pi^-\pi^0, \quad \gamma p \to \Delta^+\pi^+\pi^-, \quad \gamma p \to \Delta^0\pi^+\pi^0;$$

(c) ρ production,

$$\gamma p \to p\pi^+\rho^-, \quad \gamma p \to p\pi^0\rho^0, \quad \gamma p \to p\pi^-\rho^+;$$

(d)

$$\gamma p \to p\eta, \quad \gamma p \to p\omega, \quad \text{and} \quad \gamma p \to p\pi^+\pi^-\pi^0$$

(Lorentz-invariant phase space).

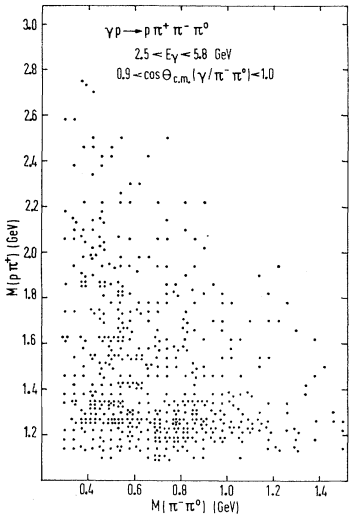

FIG. 8. Reaction $\gamma p \to p\pi^+\pi^-\pi^0$. Effective masses $M(p\pi^+)$ versus $M(\pi^-\pi^0)$ for $2.5<E_\gamma<5.8$ GeV and $0.9<\cos\theta_{\text{c.m.}}(\gamma/\pi^-\pi^0)<1.0$.

In the fit, the amounts of η and ω production were kept fixed and put equal to the values determined in Ref. 1. Details of the fitting procedure are described in the Appendix.

The curves in Figs. 2–7 show the sum of all contributions. In general, the agreement is satisfactory. A somewhat better description of the mass distributions $M(\pi^+\pi^-)$ above $E_\gamma=1.8$ GeV is obtained[13] if a contribution from the reaction $\gamma p \to \Delta^+\omega \to (p\pi^0)(\pi^+\pi^-\pi^0)$ (analyzed as $\gamma p \to p\pi^+\pi^-\pi^0$) is assumed, and if the cross section for this process is of the order as predicted by the one-pion exchange (OPE) model. Nonresonant contributions of the reactions $\gamma p \to p\pi^+\pi^-\pi^0\pi^0$ and $\gamma p \to p\pi^+\pi^-\pi^0\pi^0\pi^0$ (analyzed as $\gamma p \to p\pi^+\pi^-\pi^0$) were also tried, assuming cross sections of the order as predicted by Satz (see Sec. III A), but they did not improve the quality of the fits. The resulting cross sections for the processes (a) to (c) are compiled in Table II for different photon-energy intervals. Similar results were obtained by a least-squares fitting method.[13]

C. Reaction $\gamma p \to \Delta\rho$

The shaded areas of Fig. 2 show the $p\pi^+$ mass distributions for events with the $\pi^-\pi^0$ mass in the ρ region $[0.63<M(\pi^-\pi^0)<0.89$ GeV$]$; the shaded areas of Fig. 5 show the $\pi^-\pi^0$ mass distributions for events with the $p\pi^+$ mass in the isobar region $[1.10<M(p\pi^+)<1.34$ GeV$]$. Figure 8 gives the scatter plot of the $p\pi^+$ mass versus the $\pi^-\pi^0$ mass for all events with photon energy $2.5<E_\gamma<5.8$ GeV, which are produced at small production angles: $\cos\theta_{\text{c.m.}}>0.9$, where $\theta_{\text{c.m.}}$ is the c.m. production angle between incoming photon and outgoing $\pi^-\pi^0$ system. These distributions suggest the presence of the reaction

$$\gamma p \to \Delta^{++}\rho^-. \qquad (1')$$

The cross sections for reaction (1′), as obtained from the maximum-likelihood fit (Table II), were checked with least-square fits to the $p\pi^+$ mass distributions for events in the ρ^- region, and to the $\pi^-\pi^0$ mass distributions for events in the Δ^{++} region (shaded histogram in Figs. 2 and 5).[13]

We studied a possible contamination of reaction (1′) by events of the reaction $\gamma p \to \Delta^{++}\rho^-\pi^0$, analyzed as $\gamma p \to p\pi^+\pi^-\pi^0$. As described in Sec. II, these events

[13] P. Seyboth, thesis, Universität München, 1968 (unpublished).

would lead to a broad shoulder in the $\pi^-\pi^0$ mass distribution. We estimate the contribution of $\gamma p \to \Delta^{++}\rho^-\pi^0$ to the measured cross section for (1′) to be less than 10%.

Figure 9(a) gives the resulting total cross section for reaction (1′) as a function of the photon energy. It shows a steep rise above the threshold and a slow descent ($\sigma \sim E_\gamma^{-1.2\pm0.2}$). According to the compilation of Morrison,[14] one expects an energy dependence as $\sigma \sim E_\gamma^{-1.6}$ for OPE processes. The differential cross section $d\sigma/d\Omega$ in the c.m. system for reaction (1′) is shown in Figs. 9(b) and 9(c) for two photon-energy intervals. The values were obtained by fitting the likelihood function mentioned above to all events within certain intervals of $\cos\theta_{\text{c.m.}}$. Figure 9(c) indicates that reaction (1′) prefers small forward-production angles for photon energies above 2.5 GeV.

Photoproduction of charged ρ mesons cannot proceed via a diffraction mechanism, whereas OPE is allowed. The OPE cross section is proportional to the $\rho^- \to \pi^-\gamma$ decay width $\Gamma(\rho^- \to \pi^-\gamma)$. In order to obtain an upper limit for this width we may assume that OPE is responsible for the entire cross section observed at small production angles: $0.85 < \cos\theta_{\text{c.m.}} < 1.0$ [$\cos\theta_{\text{c.m.}} = 0.85$ corresponds to $\Delta^2(p/\Delta^{++}) \approx 0.5$ GeV^2 for $E_\gamma = 5$ GeV, where $\Delta^2(p/\Delta^{++})$ is the square of the four-momentum transfer between incoming proton and Δ^{++}]. In addition, the $p\pi^+$ and $\pi^-\pi^0$ masses were restricted to small bands around the resonance masses [$1.12 < M(p\pi^+) < 1.32$ GeV and $0.68 < M(\pi^-\pi^0) < 0.84$ GeV], where the shape of the resonance is better known than in the regions far away. With these restrictions, the cross section for (1′) was determined by a maximum-likelihood fit as described above. Figure 10 shows the resulting cross section together with the OPE prediction. In the calculation of the latter, the same restrictions in the production angle and the masses were used. The OPE cross section was calculated using form factors and off-shell corrections as proposed by Dürr and Pilkuhn.[15,16] The unknown decay width $\Gamma(\rho^- \to \pi^-\gamma)$, which enters the OPE calculation, was obtained from a best fit to the experimental cross section of Fig. 10. The resulting value was $\Gamma(\rho^- \to \pi^-\gamma) = 0.19 \pm 0.04$ MeV. Since we cannot prove (even with the restriction made for the production angle) that OPE is the only mechanism contributing to reaction (1′), the obtained value must be regarded as an upper limit: with 90% confidence level $\Gamma(\rho^- \to \pi^-\gamma) < 0.24$ MeV. The use of form factors and off-mass-shell corrections according to Ferrari and Selleri, instead of those of Dürr and Pilkuhn, does not change the OPE cross section to a significant amount. On the other hand, using absorptive corrections[17] instead of form

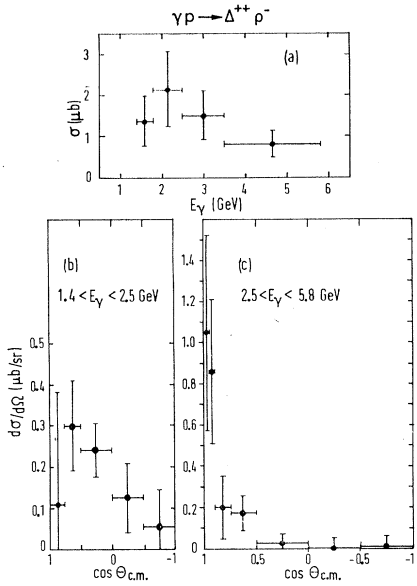

FIG. 9. Reaction $\gamma p \to \Delta^{++}\rho^-$. (a) Total cross section as function of the photon energy E_γ. (b) and (c) Differential cross section $d\sigma/d\Omega$ in the c.m. system for $1.4 < E_\gamma < 2.5$ GeV and $2.5 < E_\gamma < 5.8$ GeV.

factors, one obtains an OPE cross section that is about twice as large, and hence the value obtained for $\Gamma(\rho^- \to \pi^-\gamma)$ is smaller by a factor of 2. Our result $\Gamma(\rho^- \to \pi^-\gamma) < 0.24$ MeV is consistent with the prediction $\Gamma(\rho \to \pi\gamma) = \frac{1}{9}\Gamma(\omega \to \pi\gamma) \approx 0.1$ MeV which is obtained from SU_6 symmetry.[18,19]

The cross sections for reaction (1′) obtained by the Cambridge Bubble-Chamber Group[7] are higher than our values listed in Table II. This difference cannot be completely explained by the different fitting procedures used. The $\pi^-\pi^0$ mass distributions found in the two experiments are of different shape. Comparing the two

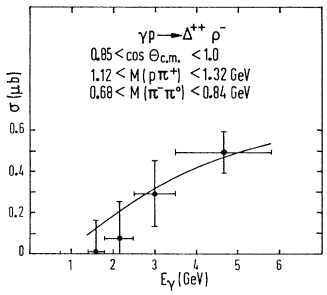

FIG. 10. Reaction $\gamma p \to \Delta^{++}\rho^-$. Cross section for small production angles ($0.85 < \cos\theta_{\text{c.m.}} < 1.0$) and small mass bands around the resonance masses [$1.12 < M(p\pi^+) < 1.32$ GeV and $0.68 < M(\pi^-\pi^0) < 0.84$ GeV]. The curve is a theoretical prediction from the OPE model for $\Gamma(\rho^- \to \pi^-\gamma) = 0.19$ MeV.

[14] D. R. O. Morrison, Phys. Letters **22**, 528 (1966).
[15] G. Wolf, Phys. Rev. Letters **19**, 925 (1967).
[16] H. P. Dürr and H. Pilkuhn, Nuovo Cimento **40**, 899 (1965).
[17] U. Maor and P. C. M. Yock, Phys. Rev. **148**, 1542 (1966); K. Schilling, DESY Report No. 66/9, 1966 (unpublished).
[18] See, for example, S. L. Glashow and R. H. Socolow, Phys. Rev. Letters **15**, 329 (1965).
[19] E. Cremmer and M. Gourdin recently estimated from a model on the cross section for $e^+e^- \to \pi^0\gamma$ the branching ratio $\Gamma(\rho^0 \to \pi^0\gamma)/\Gamma(\rho^0 \to \text{all}) = (5.5 \pm 1.1) \times 10^{-4}$, i.e., $\Gamma(\rho^0 \to \pi^0\gamma) \approx 0.06$ MeV; E. Cremmer and M. Gourdin, Nucl. Phys. **10**, B179 (1969).

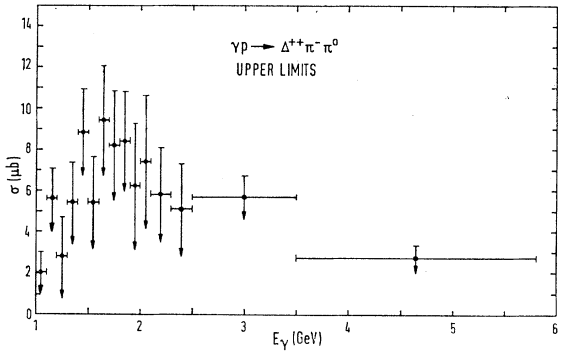

FIG. 11. Reaction $\gamma p \to \Delta^{++}\pi^-\pi^0$. Upper limit for the cross section as function of the photon energy E_γ.

experimental distributions of the $\pi^-\pi^0$ mass for $1.8<E_\gamma<2.5$ GeV, one finds a χ^2 probability of about 4% that both distributions have the same shape, and for the photon-energy interval 2.5–5.8 GeV this χ^2 probability is about 17%. Therefore, one may suppose that the differences in the cross sections for reaction (1′) from the two experiments are due to a statistical fluctuation.

Because of the small number of events observed for reaction (1′) and the strong background, it was impossible to determine the spin-density matrix elements of Δ^{++} and ρ^-. We do not find a significant amount of $\gamma p \to \Delta^+\rho^0$ and $\gamma p \to \Delta^0\rho^+$, except for a small indication for $E_\gamma>3.5$ GeV (see Table II). Using the OPE model with the relation $\Gamma(\rho^- \to \pi^-\gamma)=\Gamma(\rho^0 \to \pi^0\gamma)$ at the $\rho\pi\gamma$ vertex, and considering only the decay modes $\Delta^+ \to p\pi^0$ and $\Delta^0 \to p\pi^-$, one expects a ratio $\sigma(\gamma p \to \Delta^{++}\rho^-)$: $\sigma(\gamma p \to \Delta^+\rho^0):\sigma(\gamma p \to \Delta^0\rho^+)=9:4:1$. Our cross sections are consistent with this prediction.

D. Reaction $\gamma p \to \Delta\pi\pi$

From the maximum-likelihood fit, we also obtained information on the production of the Δ isobar in reactions where the remaining pions do not form a resonance. A relatively large cross section was found for the reaction $\gamma p \to \Delta^{++}\pi^-\pi^0$ in all energy intervals (Fig. 11 and Table II). The reaction $\gamma p \to \Delta^+\pi^+\pi^-$ is not observed at higher energies, whereas a small indication for the reaction $\gamma p \to \Delta^0\pi^+\pi^0$ is found there (see Table II). The cross sections must be regarded as upper limits because of the contamination by events with more than one π^0 as mentioned in Sec. II. The cross section for the reaction $\gamma p \to \Delta^{++}\pi^-\pi^0\pi^0$, which contaminates reaction $\gamma p \to \Delta^{++}\pi^-\pi^0$, can be estimated from the statistical model[10,11]:

$$\sigma(\gamma p \to \Delta^{++}\pi^-\pi^0\pi^0)/\sigma(\gamma p \to \Delta^{++}\pi^+\pi^-\pi^-)=0.806.$$

Using in the denominator the cross section which is reported in Sec. V, one obtains $\sigma(\gamma p \to \Delta^{++}\pi^-\pi^0\pi^0)\approx 0.9$ μb for $E_\gamma=3$ GeV and $\sigma\approx 1.5$ μb for $E_\gamma=4$ GeV.

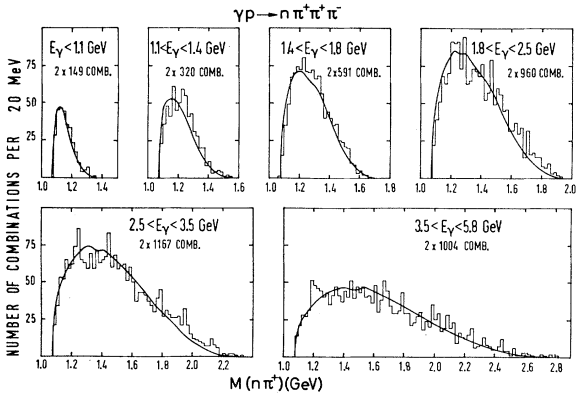

FIG. 12. Reaction $\gamma p \to n\pi^+\pi^+\pi^-$. Distributions of the $n\pi^+$ effective mass $M(n\pi^+)$ for six intervals of the photon energy. The events ambiguous between reactions $\gamma p \to n\pi^+\pi^+\pi^-$ and $\gamma p \to p\pi^+\pi^-\pi^0$ are included in Figs. 12–14. The curves are the sum of Lorentz-invariant phase space and reflection from the Δ^- resonance.

TABLE III. Reaction $\gamma p \to n\pi^+\pi^+\pi^-$. Upper limits of the cross sections (μb) for Δ^- and ρ^0 resonance production.

E_γ (GeV)	$\Delta^-\pi^+\pi^+$	$n\pi^+\rho^0$
1.1–1.4	1.0±0.6	···
1.4–1.8	5.8±0.7	···
1.8–2.5	3.5±0.7	1.3±0.9
2.5–3.5	3.9±0.7	3.8±1.1
3.5–5.8	1.9±0.4	2.1±0.7

E. Reaction $\gamma p \to p\pi\varrho$

In the fit we have looked also for the production of ρ mesons in reactions where the remaining $p\pi$ system does not form a resonance. The reaction $\gamma p \to p\pi^0\rho^0$ is observed in the ambiguous events only, and hence it may be contaminated by the reaction $\gamma p \to n\pi^+\rho^0$. Table II gives the cross sections for $\gamma p \to p\pi\rho$ in various charge states.

F. Reaction $\gamma p \to N^{*+}(1470)\varrho^0$

Since the isobar $N^{*+}(1470)(P_{11})$ has the same quantum numbers as the proton, the reaction

$$\gamma p \to N^{*+}(1470)\rho^0$$

can proceed via a diffractionlike interaction in analogy to $\gamma p \to p\rho^0$. An upper limit (with 90% confidence) of

$$\sigma(\gamma p \to N^{*+}(1470)\rho^0)<0.8\ \mu\text{b} \qquad (1'')$$
$$\searrow$$
$$p\pi^0$$

for $E_\gamma>3.5$ GeV is obtained from the likelihood fit. A similar estimate, using the decay mode $N^{*+}(1470) \to n\pi^+$, is given in Sec. IV.

IV. REACTION $\gamma p \to n\pi^+\pi^+\pi^-$

In our experiment, the sample of events of the reaction

$$\gamma p \to n\pi^+\pi^+\pi^- \qquad (2)$$

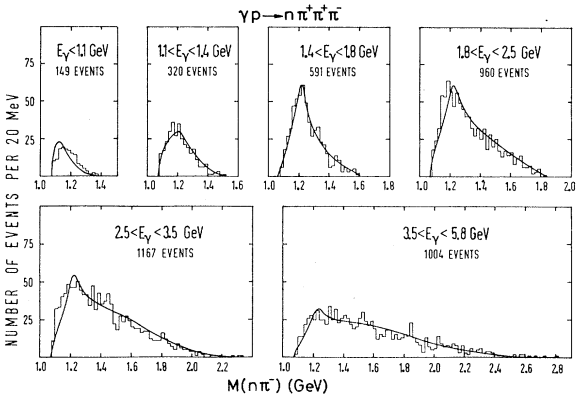

FIG. 13. Reaction $\gamma p \to n\pi^+\pi^+\pi^-$. Distributions of the $n\pi^-$ effective mass $M(n\pi^-)$. The curves are the sum of contributions from Lorentz-invariant phase space and from Δ^- resonance production.

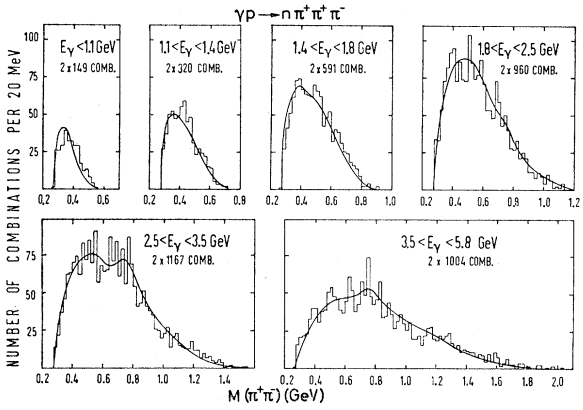

FIG. 14. Reaction $\gamma p \to n\pi^+\pi^+\pi^-$. Distributions of the $\pi^+\pi^-$ effective mass $M(\pi^+\pi^-)$. The curves are the sum of contributions from Lorentz-invariant phase space, from the process $\gamma p \to n\rho^0\pi^+$ and from $\gamma p \to \Delta^+(1236)\omega \to n\pi^+\pi^+\pi^-\pi^0$ when analyzed as $\gamma p \to n\pi^+\pi^+\pi^-$.

is contaminated by events of the type $\gamma p \to n\pi^+\pi^+\pi^- m\pi^0$, $m \geq 1$, and by events that are ambiguous between $\gamma p \to n\pi^+\pi^+\pi^-$ and $\gamma p \to p\pi^+\pi^-\pi^0$. This was discussed in Sec. II. Therefore, only upper limits could be determined for the cross section of reaction (2). They have been given in Ref. 1. Recent measurements with known photon energy yielded $\sigma(\gamma p \to n\pi^+\pi^+\pi^-) \approx 16\ \mu$b for $1.5 < E_\gamma < 3.5$ GeV, and $\sigma \approx 11\ \mu$b for $3.5 < E_\gamma < 5.3$ GeV.[8,9] An estimate for the cross sections of multineutral reactions can be obtained by the method of Satz[10,11] (see Sec. III A):

$$\sigma(\gamma p \to n\pi^+\pi^+\pi^-\pi^0)/\sigma(\gamma p \to p\pi^+\pi^+\pi^-\pi^-) = 1.8\,,$$

$$\sigma(\gamma p \to n\pi^+\pi^+\pi^-\pi^0\pi^0)/\sigma(\pi^+ p \to p\pi^+\pi^+\pi^+\pi^-\pi^-) = 0.0071\,.$$

Inserting in the denominators the values measured in this experiment (Sec. V) and in Ref. 12, one calculates for $E_\gamma = 4$ GeV

$$\sigma(\gamma p \to n\pi^+\pi^+\pi^-\pi^0) = 10 \pm 1\ \mu\text{b}\,,$$
$$\sigma(\gamma p \to n\pi^+\pi^+\pi^-\pi^0\pi^0) = 1.8 \pm 0.3\ \mu\text{b}\,.$$

Figures 12–14 show the $n\pi^+$, $n\pi^-$, and $\pi^+\pi^-$ mass distributions of reaction (2) for six intervals of the photon energy. The events that are ambiguous between reactions (1) and (2) (see Table I), have been included. Production of $\Delta^-(1236)$ and ρ^0 is seen. A superposition of Lorentz-invariant phase space and a Breit-Wigner distribution for the Δ^- was fitted to the $n\pi^-$ mass distribution of Fig. 13. The resulting cross section for the reaction

$$\gamma p \to \Delta^-\pi^+\pi^+ \qquad (2')$$

is given in Table III and in Fig. 15(a) as function of the photon energy. As discussed in Sec. II, events of the type

$$\gamma p \to \Delta^-\pi^+\pi^+\pi^0\,, \quad \searrow\ n\pi^-$$

when kinematically analyzed as $\gamma p \to n\pi^+\pi^+\pi^-$, give an enhancement in the $\Delta^-(1236)$ mass region of width 200–250 MeV. Therefore, the cross sections given for (2′) must be regarded as upper limits. The cross section for $\gamma p \to \Delta^-\pi^+\pi^+\pi^0$ can be estimated from the statistical model[10,11]:

$$\sigma(\gamma p \to \Delta^-\pi^+\pi^+\pi^0)/\sigma(\gamma p \to \Delta^{++}\pi^+\pi^+\pi^-\pi^-) = 0.9\,.$$

Using in the denominator the cross section which is given in Sec. V, one gets $\sigma(\gamma p \to \Delta^-\pi^+\pi^+\pi^0) \approx 1\ \mu$b for $E_\gamma = 3$ GeV, and $\sigma \approx 2\ \mu$b for $E_\gamma = 4$ GeV.

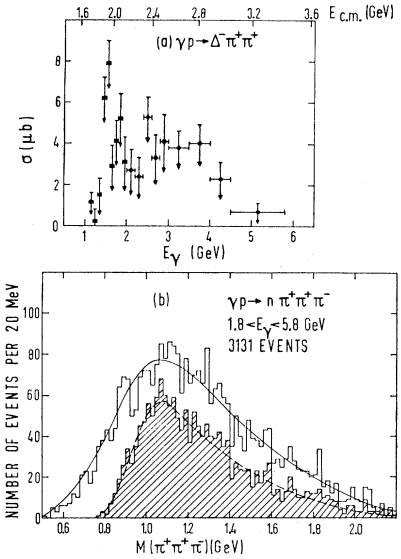

FIG. 15. (a) Reaction $\gamma p \to \Delta^-\pi^+\pi^+$. Upper limit for the cross section as function of the photon energy E_γ. $E_{\text{c.m.}}$ is the total energy in the c.m. system. (b) Reaction $\gamma p \to n\pi^+\pi^+\pi^-$. Distribution of the $\pi^+\pi^+\pi^-$ effective mass $M(\pi^+\pi^+\pi^-)$, for $1.8 < E_\gamma < 5.8$ GeV. The shaded area gives the distribution of events with at least one of the two $\pi^+\pi^-$ mass combinations lying in the ρ^0 region $0.63 < M(\pi^+\pi^-) < 0.89$ GeV. Curves show Lorentz-invariant phase space normalized to the areas.

TABLE IV. Five-prong events. Cross sections (μb) for various resonance-production processes. The columns labeled UL give upper limits for the cross sections because of contamination by multineutral events.

E_γ (GeV)	$\Delta^{++}\pi^+\pi^-\pi^-$	UL $\Delta^{++}\pi^+\pi^-\pi^-\pi^0$	UL $\Delta^0\pi^+\pi^+\pi^-\pi^0$	$p\pi^+\pi^-\rho^0$	$p\pi^+\pi^-\omega$[a]	$p\pi^+\pi^-\phi$[a]	$p\pi^+\pi^-\eta$[a]
<2.5	0.7±0.2	0.1±0.1	0.2±0.2	···	0.2±0.1	···	0.0±0.2
2.5–3.5	1.1±0.5	2.0±0.5		1.1±0.6	1.8±0.5	···	1.7±1.1
3.5–4.5	1.6±0.6	3.8±0.8	2.0±0.6	2.9±0.8	3.8±0.8	0.2±0.1	2.8±1.4
4.5–5.8	2.2±0.7	2.4±1.0		3.2±1.5	2.7±1.0	0.6±0.2	2.5±1.3

[a] Corrected for unobserved decay modes.

Figure 15(a) shows a peak in the cross section for reaction (2′) at a c.m. energy of about 1950 MeV. This could indicate the formation of the pion-nucleon resonance $\Delta(1950)$ in the s channel according to $\gamma p \to \Delta^+(1950) \to \Delta^-(1236)\pi^+\pi^+$.

In order to determine the cross section for the process

$$\gamma p \to n\pi^+\rho^0, \qquad (2'')$$

the following contributions were fitted to the $\pi^+\pi^-$ mass distributions of Fig. 14: (1) Lorentz-invariant phase space, (2) a Breit-Wigner distribution describing ρ^0 production, and (3) a contribution from events of the type $\gamma p \to \Delta^+(1236)\omega \to n\pi^+\pi^+\pi^-\pi^0$, kinematically analyzed as $\gamma p \to n\pi^+\pi^+\pi^-$. The resulting cross section for (2″) is given in Table III. The values are upper limits due to possible contamination by events of the types $\gamma p \to n\pi^+\rho^0\pi^0$ and $\gamma p \to p\pi^0\rho^0$.

The reaction

$$\gamma p \to N^{*+}(1470)\rho^0 \to (n\pi^+)(\pi^+\pi^-) \qquad (2''')$$

was not observed. This reaction should occur twice as frequently as

$$\gamma p \to N^{*+}(1470)\rho^0 \to (p\pi^0)(\pi^+\pi^-), \qquad (1'')$$

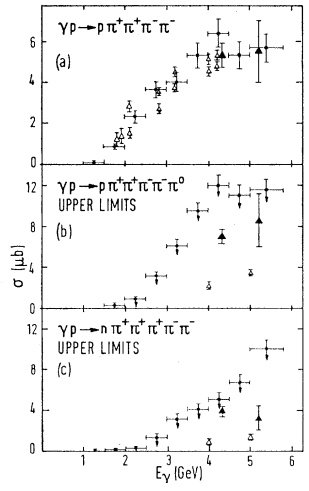

FIG. 16. Cross sections for 5-prong events as function of the photon energy E_γ. (a) Cross section for $\gamma p \to p\pi^+\pi^+\pi^-\pi^-$. (b) Upper limit of the cross section for $\gamma p \to p\pi^+\pi^+\pi^-\pi^-\pi^0$. (c) Upper limit of the cross section for $\gamma p \to n\pi^+\pi^+\pi^+\pi^-\pi^-$. Events ambiguous between $\gamma p \to p\pi^+\pi^+\pi^-\pi^-\pi^0$ and $\gamma p \to n\pi^+\pi^+\pi^+\pi^-\pi^-$ are included in both figures (b) and (c). Open triangles (△) are predictions according to Satz (Refs. 10 and 11); full triangles (▲) are measurements given in Ref. 8.

which has been discussed in Sec. III F. We get an upper limit (with 90% confidence) for the cross section

$$\sigma(\gamma p \to N^{*+}(1470)\rho^0 \to n\pi^+) < 0.9\ \mu\text{b} \quad \text{for} \quad E_\gamma > 3.5\ \text{GeV}.$$

Combining the results for (1″) and (2‴) and using the present value for the branching ratio $(N^*(1470) \to N\pi)/(N^*(1470) \to \text{all}) = 0.55$,[20] one finds for $E_\gamma > 3.5$ GeV (with 90% confidence) $\sigma(\gamma p \to N^{*+}(1470)\rho^0) < 3$ μb.

We have looked for the photoproduction of A_1^+ and A_2^+ in reaction (2). The distribution of the $\pi^+\pi^+\pi^-$ mass, $M(\pi^+\pi^+\pi^-)$, is shown in Fig. 15(b) for photon energies between 1.8 and 5.8 GeV. The dashed area gives the $\pi^+\pi^+\pi^-$ mass distribution for events with a $\pi^+\pi^-$ mass in the ρ region $[0.63 < M(\pi^+\pi^-) < 0.89\ \text{GeV}]$. Both distributions are well described by Lorentz-invariant phase space, given by the full and dashed curves, respectively. No significant production of A_1^+ and A_2^+ is seen.

V. FIVE-PRONG EVENTS

A. Cross Sections

In this section, reactions with five outgoing charged particles are discussed:

$$\gamma p \to p\pi^+\pi^+\pi^-\pi^-, \qquad (3)$$

$$\gamma p \to p\pi^+\pi^+\pi^-\pi^-\pi^0, \qquad (4)$$

$$\gamma p \to n\pi^+\pi^+\pi^+\pi^-\pi^-. \qquad (5)$$

Figure 16(a) shows the cross section for reaction (3) as function of the photon energy. The values are consistent with other bubble-chamber results[7,8] (full triangles for Ref. 8) and also with predictions using the method of Satz[10,11] [open triangles in Fig. 16(a)]. Reactions (4) and (5) are contaminated by multineutral events and by events ambiguous between (4) and (5). Thus, only upper limits could be calculated for reactions (4) and (5); they are shown in Figs. 16(b) and 16(c). From bubble-chamber experiments with known photon energies, cross sections for reactions (4) and (5) were obtained.[8] These values are given in Fig. 16(b) and 16(c) (full triangles) together with the predictions according to the method of Satz (open triangles).

[20] Particle Data Group, Rev. Mod. Phys. **41**, 109 (1969).

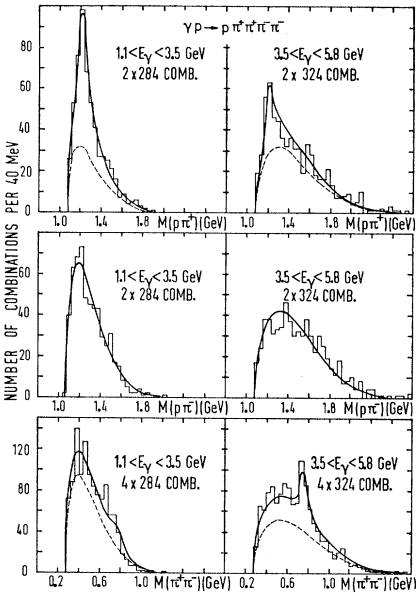

FIG. 17. Reaction $\gamma p \to p\pi^+\pi^+\pi^-\pi^-$. Distributions of the $p\pi^+$, $p\pi^-$, and $\pi^+\pi^-$ effective masses $M(p\pi^+)$, $M(p\pi^-)$, and $M(\pi^+\pi^-)$ for $1.1<E_\gamma<3.5$ GeV and $3.5<E_\gamma<5.8$ GeV. Full curves show the sum of Lorentz-invariant phase space and contributions from $\Delta^{++}(1236)$ and ρ^0 production. Dashed curves were obtained by subtracting from the full curves the contribution of Δ^{++} [for the $M(p\pi^+)$ distributions] and of ρ^0 [for the $M(\pi^+\pi^-)$ distributions], respectively.

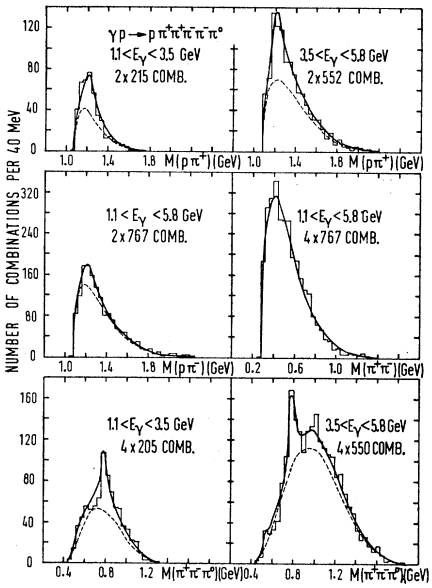

FIG. 18. Reaction $\gamma p \to p\pi^+\pi^+\pi^-\pi^-\pi^0$. Distributions of the $p\pi^+$, $p\pi^-$, $\pi^+\pi^-$, and $\pi^+\pi^-\pi^0$ effective masses, $M(p\pi^+)$, $M(p\pi^-)$, $M(\pi^+\pi^-)$, and $M(\pi^+\pi^-\pi^0)$ for various intervals of E_γ. Full curves show the sum of Lorentz-invariant phase space and contributions from the resonances $\Delta^{++}(1236)$, $\Delta^0(1236)$, ω, and η. Dashed curves were obtained by subtracting from the full curves the contribution of Δ^{++} [for the $M(p\pi^+)$ distributions], and Δ^0 [for the $M(p\pi^-)$ distribution] or of ω and η [for the $M(\pi^+\pi^-\pi^0)$ distributions]. Events ambiguous between reactions $\gamma p \to p\pi^+\pi^+\pi^-\pi^-\pi^0$ and $\gamma p \to n\pi^+\pi^+\pi^+\pi^-\pi^-$ are included. 12 events with $M(\pi^+\pi^+\pi^-\pi^-\pi^0)$ lying in the X^0 mass region are not included in the $M(\pi^+\pi^-\pi^0)$ distributions.

B. Mass Distributions and Resonance Production

Figures 17 and 18 show various two- and three-particle mass distributions of reactions (3) and (4). They give evidence for production of Δ^{++}, ρ^0, and ω, and weak indication of Δ^0 and η. Contributions of these resonances and of Lorentz-invariant phase space were simultaneously fitted to the observed mass distribution. In these fits, the effect of ρ^0 production on *all* $\pi^+\pi^-$ combinations (four combinations for each event) was taken into account, and the other resonances were treated in the analogous way. The resulting cross sections are given in Table IV; the values for ω and η production have been corrected for unobserved decay modes by a factor 1/0.9 for ω and 1/0.237 for η production. The cross sections for Δ^{++} and Δ^0 production in reaction (4) are upper limits due to contaminations by multineutral and by ambiguous events. A very large fraction of reaction (3) proceeds via production of Δ^{++} and ρ^0:

$$\gamma p \to \Delta^{++}\pi^+\pi^-\pi^- \to p\pi^+\pi^+\pi^-\pi^- \qquad (3')$$

and

$$\gamma p \to p\pi^+\pi^-\rho^0 \to p\pi^+\pi^+\pi^-\pi^-; \qquad (3'')$$

however, no significant simultaneous production of Δ^{++} and ρ^0 was found.[21,22] The cross section for reaction (3′) can be compared with the prediction, which follows from the method of Satz[10,11]:

$$\sigma(\gamma p \to \Delta^{++}\pi^+\pi^-\pi^-)/\sigma(\pi^+ p \to \Delta^{++}\pi^+\pi^-\pi^0) = 0.00167.$$

Using in the denominator the cross section given in Ref. 12, one obtains $\sigma(\gamma p \to \Delta^{++}\pi^+\pi^-\pi^-) = 1.8 \pm 0.5\ \mu$b

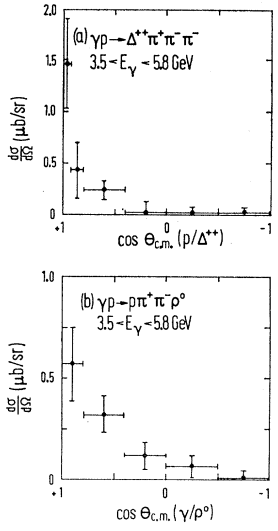

FIG. 19. Differential cross section $d\sigma/d\Omega$ in the c.m. system for $3.5<E_\gamma<5.8$ GeV, (a) for reaction $\gamma p \to \Delta^{++}\pi^+\pi^-\pi^- \to p\pi^+\pi^+\pi^-\pi^-$, (b) for reaction $\gamma p \to p\pi^+\pi^-\rho^0 \to p\pi^+\pi^+\pi^-\pi^-$.

[21] W. Tejessy, thesis, Universität Bonn, 1968 (unpublished).
[22] H. Beisel, thesis, Universität Heidelberg, 1968 (unpublished).

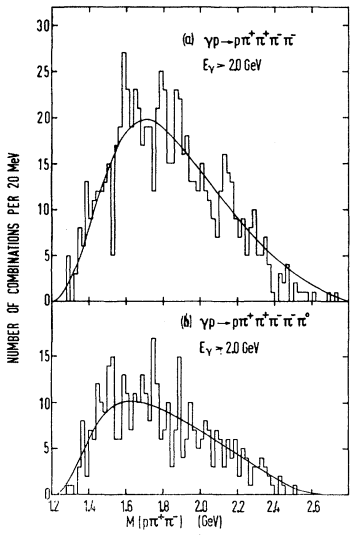

FIG. 20. (a) Reaction $\gamma p \to p\pi^+\pi^+\pi^-\pi^-$. Distribution of the $p\pi_a^+\pi_a^-$ effective mass $M(p\pi_a^+\pi_a^-)$, for events with $M(\pi_b^+\pi_b^-)$ in the ρ^0 mass region $0.63<M(\pi_b^+\pi_b^-)<0.89$ GeV and for $E_\gamma>2$ GeV. (b) Reaction $\gamma p \to p\pi^+\pi^+\pi^-\pi^-\pi^0$. Distribution of the $p\pi_a^+\pi_a^-$ effective mass $M(p\pi_a^+\pi_a^-)$, for events with $M(\pi_b^+\pi_b^-\pi^0)$ in the ω mass region $0.763<M(\pi_b^+\pi_b^-\pi^0)<0.803$ GeV and for $E_\gamma>2$ GeV. The curves show Lorentz-invariant phase space normalized to the total number of events.

for $E_\gamma=4$ GeV. The prediction is consistent with the value given in Table IV for $3.5<E_\gamma<4.5$ GeV.

The differential cross sections $d\sigma/d\Omega$ for reactions (3′) and (3″) are given in Figs. 19(a) and 19(b). They were determined by dividing the data into bins of the production angle and then fitting the resonance fraction. Figure 19 shows that small production angles are preferred.

The ω meson is observed in reaction (4):

$$\gamma p \to p\pi^+\pi^-\omega \to p\pi^+\pi^+\pi^-\pi^-\pi^0.$$

Because of the large background, the production and decay angular distributions of the ω could not be determined. No significant simultaneous production of Δ^{++} and ω was found in reaction (4).[21,22] Also, no obvious evidence was observed for reactions of the type $\gamma p \to N^{*+}\rho^0 \to (p\pi^+\pi^-)(\pi^+\pi^-)$ or $\gamma p \to N^{*+}\omega \to (p\pi^+\pi^-)(\pi^+\pi^-\pi^0)$ (N^{*+} designates a pion-nucleon resonance decaying into $p\pi^+\pi^-$). This can be seen from Fig. 20, where the invariant mass $M(p\pi^+\pi^-)$ is shown (a) for reaction (3) with the invariant mass of the remaining two pions lying in the ρ^0 region, and (b) for reaction (4) with the invariant mass of the remaining three pions in the ω region.

Δ^{++}, ρ^0, and ω production in reactions (3) and (4) was also observed by Eisenberg *et al.* at 4.3-GeV photon energy.[8] They obtained cross sections consistent with ours.

In reaction (5), no significant resonance production is observed. The effective-mass distributions given in Fig. 21 are well described by Lorentz-invariant phase space.

For all five-prong events, the assignment to reaction

$$\gamma p \to p\pi^+\pi^-K^+K^- \tag{6}$$

was tried. Twenty-five events were found to be kinematically, as well as according to ionization, consistent with this reaction; these events could be uniquely assigned to (6). Figure 22(a) shows the cross section and Fig. 22(b) shows the K^+K^- mass distribution for reaction (6). There is slight evidence for ϕ meson production via $\gamma p \to p\pi^+\pi^-\phi \to p\pi^+\pi^-(K^+K^-)$. Additional evidence comes from events of the type

$$\gamma p \to p\pi^+\pi^-K^0\bar{K}^0, \tag{7}$$

with one visible K^0 decay. The $K^0\bar{K}^0$ mass distribution, which is also shown in Fig. 22(b), contains a ϕ peak as well. The heights of the ϕ peaks in the K^+K^- and $K^0\bar{K}^0$ mass distribution are consistent with the known branching ratio $\Gamma(\phi \to K^+K^-)/\Gamma(\phi \to K_L^0K_S^0)\approx 1.45$.[20] The production angular distribution in the c.m. system for events in the ϕ region [$1.00<M(K\bar{K})<1.04$ GeV] is shown in Fig. 22(c), which indicates that small production angles are preferred. Cross sections for the production of the three vector mesons ρ^0, ω, and ϕ have already been given in Ref. 4.

Production of X^0 in reaction $\gamma p \to pX^0 \to p\pi^+\pi^-\eta \to p\pi^+\pi^-(\pi^+\pi^-\pi^0)$ has been found and was discussed in Ref. 1. Removing from the $\pi^+\pi^-\pi^0$ mass distribution all events which have a $\pi^+\pi^+\pi^-\pi^-\pi^0$ mass in the X^0 region, one still sees a shoulder at the mass of the η meson (see Fig. 18 for $3.5<E_\gamma<5.8$ GeV). This shows that the η meson is also produced directly in the reaction $\gamma p \to p\pi^+\pi^-\eta$. The corresponding cross section is given in Table IV.

C. An Upper Limit for the Decay $\rho^0 \to \pi^+\pi^+\pi^-\pi^-$

A total of 1550 ρ^0 mesons in the mass region $M(\pi^+\pi^-)<900$ MeV was observed in the reaction $\gamma p \to p\pi^+\pi^-$

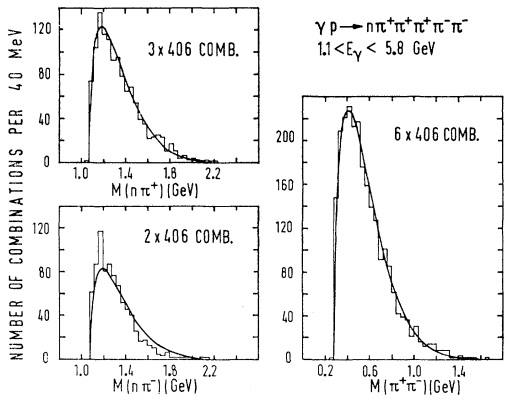

FIG. 21. Reaction $\gamma p \to n\pi^+\pi^+\pi^+\pi^-\pi^-$. Distributions of the $n\pi^+$, $n\pi^-$, and $\pi^+\pi^-$ effective masses $M(n\pi^+)$, $M(n\pi^-)$, and $M(\pi^+\pi^-)$ for $1.1<E_\gamma<5.8$ GeV. The curves show Lorentz-invariant phase space normalized to the total number of events. Events ambiguous between reactions $\gamma p \to n\pi^+\pi^+\pi^+\pi^-\pi^-$ and $\gamma p \to p\pi^+\pi^+\pi^-\pi^-\pi^0$ are included.

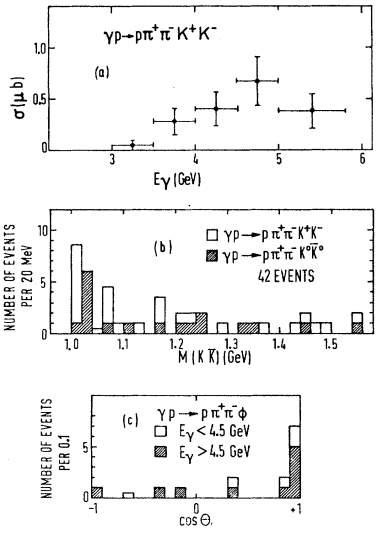

FIG. 22. Reaction $\gamma p \to p\pi^+\pi^- K\bar{K}$. (a) Cross section for reaction $\gamma p \to p\pi^+\pi^- K^+K^-$. (b) Distributions of the K^+K^- effective mass, $M(K^+K^-)$, from reaction $\gamma p \to p\pi^+\pi^- K^+K^-$ (unshaded) and of the $K^0\bar{K}^0$ effective mass, $M(K^0\bar{K}^0)$, from reaction $\gamma p \to p\pi^+\pi^- K^0\bar{K}^0$ (shaded). (c) Distribution of the production angle $\cos\theta_{\text{c.m.}}(\gamma/\phi)$ in the c.m. system for $\gamma p \to p\pi^+\pi^-\phi$ for $E_\gamma<4.5$ GeV (unshaded) and $E_\gamma>4.5$ GeV (shaded). All events of reactions $\gamma p \to p\pi^+\pi^- K^+K^-$ and $\gamma p \to p\pi^+\pi^- K^0\bar{K}^0$ are taken with $M(K\bar{K})$ in the ϕ mass region $1.00<M(K\bar{K})<1.04$ GeV.

for $E_\gamma>2.5$ GeV (see Ref. 1). We have looked for the decay $\rho^0 \to \pi^+\pi^+\pi^-\pi^-$ in the reaction $\gamma p \to p\pi^+\pi^+\pi^-\pi^-$. No event was found in the mass region $M(\pi^+\pi^+\pi^-\pi^-)<900$ MeV. This leads to the following upper limit (90% confidence):

$$\Gamma(\rho^0 \to \pi^+\pi^+\pi^-\pi^-)/\Gamma(\rho^0 \to \pi^+\pi^-)<0.0015.$$

D. $I=\frac{5}{2}$ Mass Distributions

Combining the $p\pi^+\pi^+$ and $n\pi^-\pi^-$ mass distributions from reactions (3), (4), and (5) [Figs. 23(a)–23(c)], one gets the $I=\frac{5}{2}$ mass distribution shown in Fig. 23(d). It has a slight peak above background near 1550 MeV. On the other hand, the combined $p\pi^+\pi^-$ and $n\pi^+\pi^-$ mass distribution, which presumably contains a smaller contribution of $I=\frac{5}{2}$, does not show such a peak [see Fig. 23(e)]. This could be an indication for production of an $I=\frac{5}{2}$ baryon resonance with mass about 1550 MeV. A similar enhancement has been found, at the same mass, by the Cambridge Bubble-Chamber Collaboration.[7] In our data, the effect is seen mainly in reaction (5) [see Fig. 23(c)], which may be strongly contaminated by multineutral events and by events that are ambiguous between reactions (4) and (5).

VI. MASS DEPENDENCE OF DIFFERENTIAL CROSS SECTIONS

For each of the reactions

$$\gamma p \to p\pi^+\pi^-\pi^0, \quad (1)$$

$$\gamma p \to n\pi^+\pi^+\pi^-, \quad (2)$$

$$\gamma p \to p\pi^+\pi^+\pi^-\pi^-, \quad (3)$$

$$\gamma p \to p\pi^+\pi^+\pi^-\pi^-\pi^0, \quad (4)$$

$$\gamma p \to n\pi^+\pi^+\pi^+\pi^-\pi^-, \quad (5)$$

we examined the differential cross section $d\sigma/d\Delta'^2$ for different values of the invariant mass M of all pions. Here $\Delta'^2=\Delta^2-\Delta^2_{\min}(M)$, Δ^2 is the square of the four-momentum transfer between the initial and the final nucleon, and $\Delta^2_{\min}(M)$ is the minimum value of Δ^2, that is kinematically allowed for a given value of M.

For different values of M, an expression of the form

$$d\sigma/d\Delta'^2=C(M)e^{-A(M)\Delta'^2}$$

was fitted to the differential cross sections, using all events with $3.5<E_\gamma<5.8$ GeV and $0<\Delta'^2<1.2$ GeV^2. Figures 24(a)–24(e) show for each of the reactions (1)–(5) the slope $A(M)$ as a function of the mass M of all pions. One sees that, in general, the slope decreases with increasing M. This feature has also been observed in recent π^+p and K^-p experiments with three or more final particles[23,24] and in this experiment for the reaction $\gamma p \to p\pi^+\pi^-$.[1] Comparing the distributions of $A(M)$ versus M for the different reactions (1)–(5), one finds

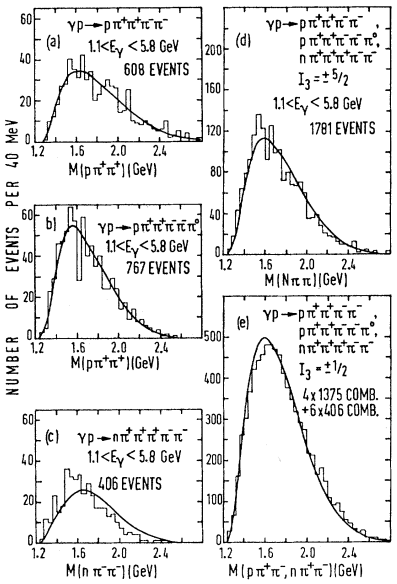

FIG. 23. (a) Distribution of the $p\pi^+\pi^+$ effective mass $M(p\pi^+\pi^+)$, for reaction $\gamma p \to p\pi^+\pi^+\pi^-\pi^-$. (b) Distribution of the $p\pi^+\pi^+$ effective mass $M(p\pi^+\pi^+)$, for reaction $\gamma p \to p\pi^+\pi^+\pi^-\pi^-\pi^0$. (c) Distribution of the $n\pi^-\pi^-$ effective mass $M(n\pi^-\pi^-)$, for reaction $\gamma p \to n\pi^+\pi^+\pi^+\pi^-\pi^-$. (d) Sum of the distributions (a), (b), and (c) (isospin $I=\frac{5}{2}$). (e) Sum of the distributions $M(p\pi^+\pi^-)$ and $M(n\pi^+\pi^-)$ for reactions $\gamma p \to p\pi^+\pi^+\pi^-\pi^-$, $\gamma p \to p\pi^+\pi^+\pi^-\pi^-\pi^0$, and $\gamma p \to n\pi^+\pi^+\pi^+\pi^-\pi^-$ (isospin $I=\frac{1}{2}, \frac{3}{2}, \frac{5}{2}$ is possible). The curves are the sum of Lorentz-invariant phase space and the contributions from the processes listed in Table IV.

[23] Aachen-Berlin-CERN-London (I.C.)-Vienna Collaboration, Phys. Letters **27B**, 336 (1968).
[24] G. Cocconi, Nuovo Cimento **57A**, 837 (1968).

TABLE V. Cross section for reaction $\gamma p \to pK^+K^-$.

E_γ (GeV)	1.58–2.0	2.0–2.5	2.5–3.0	3.0–3.5	3.5–4.0	4.0–4.5	4.5–5.0	5.0–5.8
σ (μb)	0.21±0.07	0.47±0.12	0.54±0.14	1.06±0.23	0.64±0.19	0.97±0.26	1.11±0.30	0.92±0.26

that the decrease of the slope $A(M)$ with increasing M becomes less pronounced with increasing multiplicity. One has to keep in mind, however, that reactions (1), (2), (4), and (5) are contaminated by multineutral and ambiguous events, which could influence the numerical values obtained for $A(M)$.

VII. PRODUCTION OF STRANGE PARTICLES

A. Experimental Details

Preliminary results on the photoproduction of strange particles, based on part of the statistics, have been published in Ref. 3. The results presented below refer to a final sample of 1185 events with at least one visible strange-particle decay and on 107 pK^+K^- events with no visible decay. The pK^+K^- events were selected on the basis of kinematics and of ionization. Only eight of the 107 pK^+K^- events were ambiguous with the hypothesis $p\pi^+\pi^-$. Results on the reactions $\gamma p \to pK^+K^-$ and $\gamma p \to pK^0\bar{K}^0$ have been reported in connection with ϕ production via $\gamma p \to p\phi$ in Refs. 1 and 4, except for the cross section of reaction $\gamma p \to pK^+K^-$, which is given in Table V.

Table VI gives for all observed reactions the number of unique events (column A) and the total number of events after apportionment of the ambiguous ones (column B). Column B also contains 60 events which had been identified as strange-particle events in the scanning procedure but which were unmeasurable or did not successfully fit any of the kinematically possible interpretations.

The following acceptance criteria for the hypotheses were used: (a) compatibility of the observed bubble density with the bubble density calculated by GRIND, (b) a 3-constraint (3-C) fit was preferred to 0-C and 1-C fits. In particular, FAKE[25] calculations for one-prong events with a visible Λ decay showed that ΛK^+ is the correct hypothesis whenever it is fitted by GRIND. Most of the ambiguous events (e.g., ambiguous between reactions $\gamma p \to \Lambda K^0\pi^+$ and $\gamma p \to \Lambda K^+\pi^0$ with visible Λ decay) could be apportioned by starting for each reaction with those topologies in which the reaction could be identified uniquely (e.g., $\gamma p \to \Lambda K^0\pi^+$ with visible Λ *and* K^0 decays). From there the number of events with other topologies was estimated for each reaction.

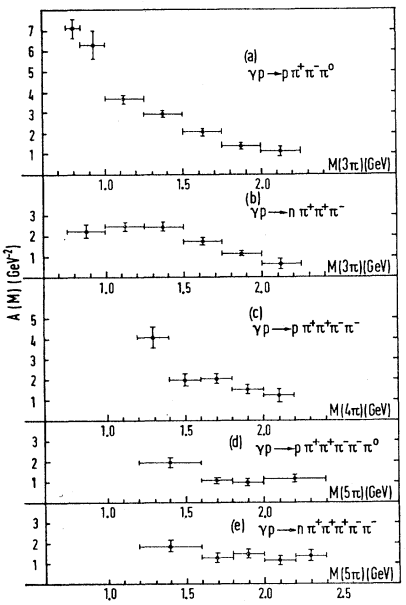

FIG. 24. Slope $A(M)$ of the differential cross section $d\sigma/d\Delta'^2 = Ce^{-A(M)\Delta'^2}$ for $3.5 < E_\gamma < 5.8$ GeV as function of the effective mass M of all pions, for the reactions (a) $\gamma p \to p\pi^+\pi^-\pi^0$, (b) $\gamma p \to n\pi^+\pi^+\pi^-$, (c) $\gamma p \to p\pi^+\pi^+\pi^-\pi^-$, (d) $\gamma p \to p\pi^+\pi^+\pi^-\pi^-\pi^0$, (e) $\gamma p \to n\pi^+\pi^+\pi^+\pi^-\pi^-$.

TABLE VI. Number of events with at least one visible strange-particle decay. (A) Number of unique events. (B) Number of events after apportionment of the ambiguous events.

Reaction	A	B	Reaction	A	B
ΛK^+	170	186	$\Sigma^+K^+\pi^-\pi^0(\pi^0\cdots)$	16	31
Σ^+K^0	6	18	$\left\{\begin{matrix}\Sigma^0\\ \Lambda\end{matrix}\right\}K^0\pi^+\pi^0(\pi^0\cdots)$	24	107
Σ^0K^+	25	102	$\Sigma^-K^+\pi^+\pi^0(\pi^0\cdots)$	4	13
pK^+K^-	5	5	$\Xi^-K^+\bar{K}^0\pi^+(\pi^0\cdots)$	1	1
$pK^0\bar{K}^0(\pi^0\cdots)$	4	31	$pK^+K^-\pi^+\pi^-$	3	5
$\Lambda K^0\pi^+$	29	122	$\Lambda K^0\pi^+\pi^+\pi^-$	2	7
$\Sigma^+K^+\pi^-$	50	54	$\Sigma^-K^+\pi^+\pi^+\pi^-$	1	1
$\Sigma^0K^0\pi^+$	4	16	$pK^+\bar{K}^0\pi^-\pi^0(\pi^0\cdots)$	1	4
$\Sigma^-K^+\pi^+$	33	34	$pK^0\bar{K}^0\pi^+\pi^-(\pi^0\cdots)$	7	18
$nK^+\bar{K}^0(\pi^0\cdots)$	9	23	$pK^0K^-\pi^+\pi^0(\pi^0\cdots)$	3	5
$\Sigma^+K^0\pi^0(\pi^0\cdots)$	6	18	$nK^+\bar{K}^0\pi^+\pi^-(\pi^0\cdots)$	2	6
$\left\{\begin{matrix}\Sigma^0\\ \Lambda\end{matrix}\right\}K^+\pi^0(\pi^0\cdots)$	69	173	$nK^0K^-\pi^+\pi^+(\pi^0\cdots)$	1	3
$pK^+\bar{K}^0\pi^-$	4	8	$\Sigma^+K^0\pi^+\pi^-\pi^0(\pi^0\cdots)$	1	19
$pK^0K^-\pi^+$	14	19	$\left\{\begin{matrix}\Sigma^0\\ \Lambda\end{matrix}\right\}K^+\pi^+\pi^-\pi^0(\pi^0\cdots)$	8	23
$\Lambda K^+\pi^+\pi^-$	28	38			
$\Sigma^+K^0\pi^+\pi^-$	3	13	$\left\{\begin{matrix}\Sigma^0\\ \Lambda\end{matrix}\right\}K^0\pi^+\pi^+\pi^-\pi^0(\pi^0\cdots)$	···	21
$\Sigma^0K^+\pi^+\pi^-$	5	6	$\Sigma^-K^0\pi^+\pi^+\pi^0(\pi^0\cdots)$	4	13
$\Sigma^-K^0\pi^+\pi^+$	···	10	$pK^+K^-\pi^+\pi^-\pi^0(\pi^0\cdots)$	1	2
$pK^0\bar{K}^0\pi^0(\pi^0\cdots)$	1	5	$nK^0\bar{K}^0\pi^+\pi^+\pi^-(\pi^0\cdots)$	1	1
$nK^+K^-\pi^+(\pi^0\cdots)$	5	7	$\Sigma^+K^0\pi^+\pi^+\pi^-\pi^-(\pi^0\cdots)$	1	5
$nK^0\bar{K}^0\pi^+(\pi^0\cdots)$	2	12			
Sum					1185
with no visible decay:					
pK^+K^-					107
$pK^+\pi^-\pi^+\pi^-$					20
Sum					1312

[25] G. R. Lynch, University of California Lawrence Radiation Laboratory Report No. UCRL-10335 (unpublished); H. Kübeck and E. Raubold, revised version of FAKE, DESY, FAKE manual, 1969 (unpublished).

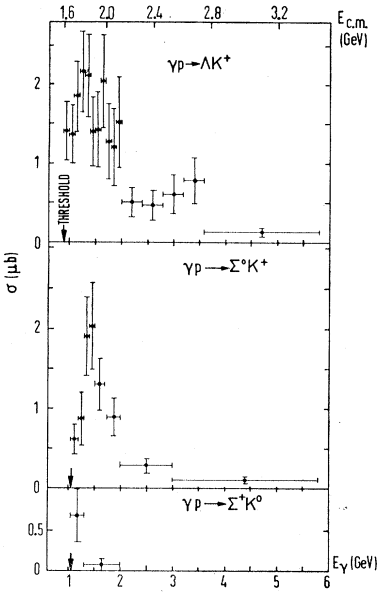

FIG. 25. Reactions $\gamma p \to \Lambda K^+$, $\Sigma^0 K^+$, and $\Sigma^+ K^0$. Cross sections as functions of the photon energy. $E_{c.m.}$ is the total energy in the c.m. system.

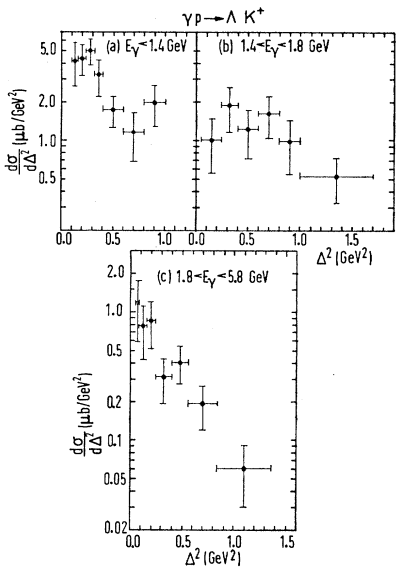

FIG. 27. Reaction $\gamma p \to \Lambda K^+$. Differential cross section $d\sigma/d\Delta^2$ as function of Δ^2 for three photon-energy intervals. Δ^2 is the square of the four-momentum transfer between photon and K^+ meson.

An exception was made for the 1-C fit $\gamma p \to \Sigma^0 K^+ \to \Lambda\gamma K^+$ with visible Λ decay. From the results of FAKE calculations, we concluded that for $E_\gamma < 2$ GeV about 10% of all events fitting the $\Sigma^0 K^+$ hypothesis really were events of the reaction $\Lambda K^+\pi^0$ (0-C), and for $E_\gamma > 2$ GeV about 50% of all events fitting the $\Sigma^0 K^+$ hypothesis really were events of the reactions $\Lambda K^+\pi^0$ and $\Lambda K^0\pi^+$ (0-C). The separation of the $\Sigma^0 K^+$ events from the $\Lambda K^+\pi^0$ and $\Lambda K^0\pi^+$ events could therefore only be done by a statistical method with help of the FAKE results.

The following reactions have been studied:

$$\gamma p \to \Lambda K^+, \tag{8}$$

$$\gamma p \to \Sigma^0 K^+, \tag{9}$$

$$\gamma p \to \Sigma^+ K^0, \tag{10}$$

$$\gamma p \to \Lambda K^+ \pi^0 (\pi^0 \cdots), \tag{11}$$

$$\gamma p \to \Lambda K^0 \pi^+ (\pi^0 \cdots), \tag{12}$$

$$\gamma p \to \Sigma^+ K^+ \pi^-, \tag{13}$$

$$\gamma p \to \Sigma^- K^+ \pi^+, \tag{14}$$

$$\gamma p \to \Lambda K^+ \pi^+ \pi^-, \tag{15a}$$

and

$$\gamma p \to \Lambda K^+ \pi^+ \pi^- \pi^0 (\pi^0 \cdots). \tag{15b}$$

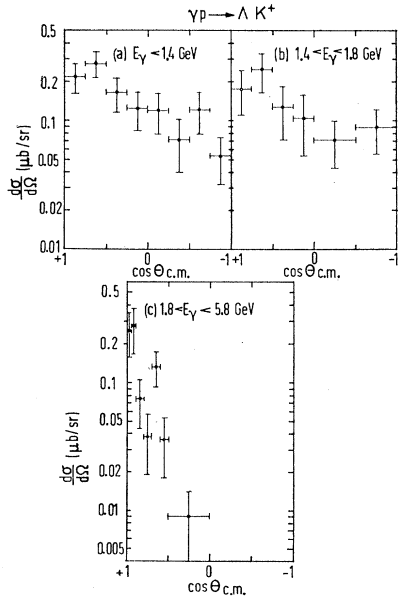

FIG. 26. Reaction $\gamma p \to \Lambda K^+$. Differential cross sections $d\sigma/d\Omega$ (in the c.m. system) as a function of $\cos\theta_{c.m.}$ for three photon-energy intervals. $\theta_{c.m.}$ is the angle between photon and K^+ meson in the c.m. system.

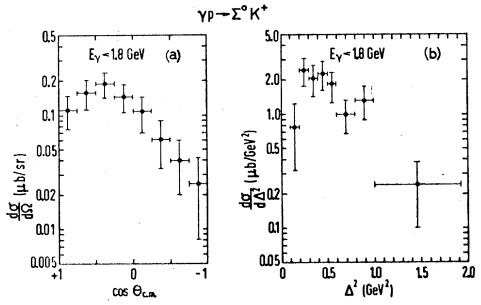

FIG. 28. Reaction $\gamma p \to \Sigma^0 K^+$. (a) Differential cross section $d\sigma/d\Omega$ as function of $\cos\theta_{c.m.}$. (b) Differential cross section $d\sigma/d\Delta^2$ as function of Δ^2. $\theta_{c.m.}$ and Δ^2 have the same meaning as in Figs. 26 and 27.

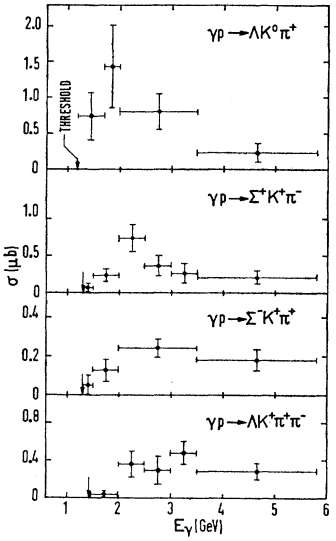

FIG. 29. Reactions $\gamma p \to \Lambda K^0\pi^+$, $\Sigma^+K^+\pi^-$, $\Sigma^-K^+\pi^+$, and $\Lambda K^+\pi^+\pi^-$. Cross sections as function of the photon energy.

For the reactions (8), (10), (12)–(15a), in general, a 3-C fit is possible, thus allowing a unique kinematical identification. For these reactions, only the 3-C fit events were used to calculate the cross sections. For reaction (9), only 1-C fits were used to calculate the cross section. In the mass distributions of reactions (11), (12), and (15), however, 0-C fit events were also included. The cross sections given below have been corrected for scanning losses (about 1–2%) and for unobserved decay modes. Furthermore they have been corrected for geometrical losses, which are due to the finite size of the bubble chamber and to very short decay lengths. The following geometrical correction factors C have been used:

For Λ, Σ^0 decay, $C=1.08$;
for K^0 decay, $C=1.11$;
for Σ^+ decay, $C=1.24$;
for Σ^- decay, $C=1.11$.

B. Cross Sections

Figure 25 shows the cross sections for reactions (8)–(10) as a function of the photon energy E_γ. Figures 26 and 27 give the differential cross sections $d\sigma/d\Omega_{\text{c.m.}}$ and $d\sigma/d\Delta^2$ for reaction (8) in three intervals of E_γ. The differential cross section $d\sigma/d\Delta^2$ for $1.8<E_\gamma<5.8$ GeV [Fig. 27(c)] was fitted to an exponential of the form $d\sigma/d\Delta^2=Ce^{-A\Delta^2}$.
The resulting values for C and A are

$$C=1.02\pm0.28\ (\mu\text{b/GeV}^2),\quad A=2.5\pm0.5\ (\text{GeV}^{-2}).$$

Figures 28(a) and 28(b) show the differential cross section for reaction (9). The cross sections for reaction (9) were calculated taking into account the FAKE results

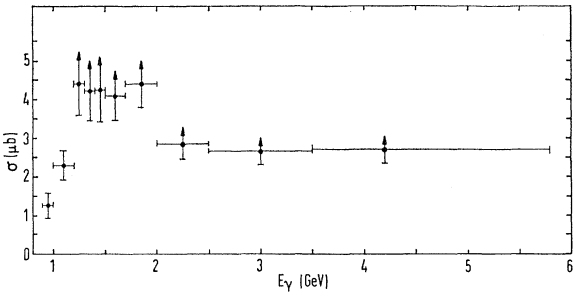

FIG. 30. Lower limit of the cross section for strange-particle production as function of the photon energy.

mentioned above. Because of large contaminations ($\approx 50\%$) from other reactions at higher energies, we could not determine the differential cross section for reaction (9) for $E_\gamma>1.8$ GeV.

Measurements of reactions (8) and (9) have been carried out by various authors at photon energies below 1.2 GeV; the results together with a summary of possible theoretical interpretations have been compiled by Grilli *et al.*[26] and Thom.[27] At higher energies, measurements have been performed by Elings *et al.* (3.4–4 GeV),[28] by the Cambridge Bubble-Chamber Group (1–5 GeV) [6] and by Boyarski *et al.* (5–16 GeV).[29] Their results are in agreement with our cross sections within the statistical accuracy.

Figure 29 shows the cross sections for reactions (12) to (15a) as a function of E_γ. Figure 30 gives the sum of the cross sections for the reactions (8)–(10), (12)–(15a), and other reactions for which the photon energy could be determined uniquely. Except for the two points

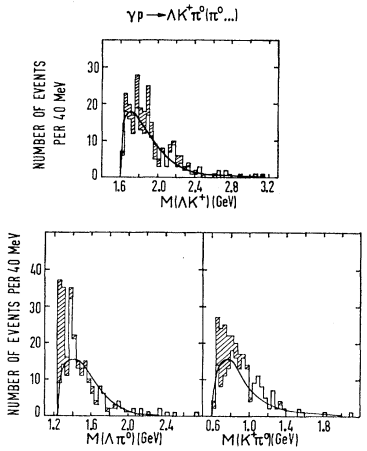

FIG. 31. Reaction $\gamma p \to \Lambda K^+\pi^0(\pi^0\cdots)$ for $E_\gamma<5.8$ GeV. Distributions of the ΛK^+, $\Lambda\pi^0$, and $K^+\pi^0$ effective masses, $M(\Lambda K^+)$, $M(\Lambda\pi^0)$, and $M(K^+\pi^0)$. All events are shown which gave a $\Lambda K^+\pi^0$ fit consistent with the observed track ionization. Shaded events are ambiguous between $\Lambda K^+\pi^0$ and Σ^0K^+. Curves are Lorentz-invariant phase space fitted to the unshaded events.

[26] M. Grilli *et al.*, Nuovo Cimento **38**, 1467 (1965).
[27] H. Thom, Phys. Rev. **151**, 1322 (1966).
[28] V. B. Elings *et al.*, Phys. Rev. Letters **16**, 474 (1966).
[29] A. M. Boyarski *et al.*, Phys. Rev. Letters **22**, 1131 (1969).

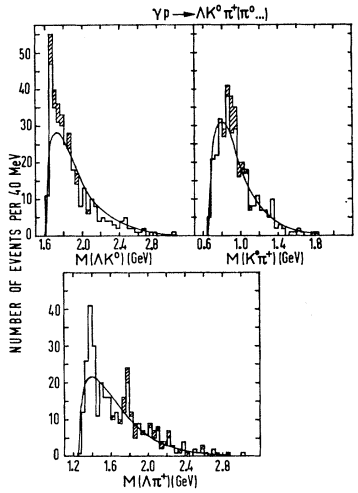

FIG. 32. Reaction $\gamma p \to \Lambda K^0\pi^+(\pi^0\cdots)$ for $E_\gamma<5.8$ GeV. Distributions of the ΛK^0, $K^0\pi^+$, and $\Lambda\pi^+$ effective masses, $M(\Lambda K^0)$, $M(K^0\pi^+)$, and $M(\Lambda\pi^+)$. All events are shown which gave a $\Lambda K^0\pi^+$ fit consistent with the observed track ionization. Shaded events are ambiguous between $\Lambda K^0\pi^+(\pi^0\cdots)$ and Σ^0K^+. Curves are Lorentz-invariant phase space fitted to the unshaded events.

with $E_\gamma<1.2$ GeV, the values given in Fig. 30 are lower limits to the cross section for strange-particle production.

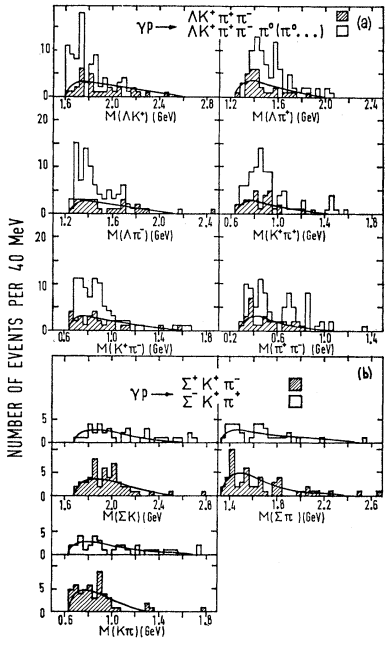

FIG. 33. (a) Reactions $\gamma p \to \Lambda K^+\pi^+\pi^-$ and $\Lambda K^+\pi^+\pi^-\pi^0(\pi^0\cdots)$ for $E_\gamma<5.8$ GeV. Distributions of the ΛK^+, $\Lambda\pi^+$, $\Lambda\pi^-$, $K^+\pi^+$, $K^+\pi^-$, and $\pi^+\pi^-$ effective masses $M(\Lambda K^+)$, $M(\Lambda\pi^+)$, $M(\Lambda\pi^-)$, $M(K^+\pi^+)$, $M(K^+\pi^-)$, and $M(\pi^+\pi^-)$. Shaded events are from reaction $\gamma p \to \Lambda K^+\pi^+\pi^-$. Curves are Lorentz-invariant phase space fitted to the shaded events. (b) Reactions $\gamma p \to \Sigma^+K^+\pi^-$ and $\Sigma^-K^+\pi^+$ for $E_\gamma<5.8$ GeV. Distributions of the ΛK, $\Sigma\pi$, and $K\pi$ effective masses $M(\Sigma K)$, $M(\Sigma\pi)$, and $M(K\pi)$. Curves show Lorentz-invariant phase space.

TABLE VII. Cross sections for $\Sigma(1385)$ production.

Reaction	Photon-energy interval (GeV)	σ (μb)
$\gamma p \to \Sigma^0(1385)K^+$	1.42–2.00	0.67±0.27
	2.00–5.80	0.15±0.09
$\gamma p \to \Sigma^+(1385)K^0$	1.42–2.00	0.68±0.48
	2.00–5.80	0.13±0.09

C. Resonance Production

Figures 31–33(a) show the distributions of the effective masses of the ΛK, $\Lambda\pi$, and $K\pi$ systems for reactions (11), (12), and (15); Fig. 33(b) gives the distribution of the ΣK, $\Sigma\pi$, and $K\pi$ effective masses for reactions (13) and (14). The events have been plotted without geometrical correction factors. In the case of reactions (11), (12), and (15), ambiguous events have also been included.

The $\Lambda\pi^0$ mass distribution of reaction (11) in Fig. 31 shows, at masses below 1.32 GeV, a strong accumulation of events, which are ambiguous between reactions $\gamma p \to \Lambda K^+\pi^0(\pi^0\cdots)$ and $\gamma p \to \Sigma^0K^+$ (shaded events). FAKE calculations showed that nearly all of these events really belong to reaction Σ^0K^+. The unshaded $\Lambda\pi^0$ mass distribution in Fig. 31 gives evidence for $\Sigma^0(1385)$ production in reaction (11). Owing to the following reason, the events in the $\Sigma^0(1385)$ peak belong to the reaction with only one π^0 in the final state: Events of the reaction with two neutral pions $\gamma p \to \Sigma^0(1385)K^+\pi_2^0 \to (\Lambda\pi_1^0)K^+\pi_2^0$ are analyzed in GRIND as $\gamma p \to \Lambda K^+\pi^0$, with a fictitious π^0 substituted for the neutral $\pi_1^0\pi_2^0$ system. The $\Lambda\pi^0$ effective mass of these events will not have a $\Sigma^0(1385)$ peak. Therefore the events in the $\Sigma^0(1385)$ peak of Fig. 31 come from reaction

$$\gamma p \to \Sigma^0(1385)K^+ \to \Lambda\pi^0K^+. \qquad (11')$$

The resulting cross section for (11′), corrected for unobserved decay modes, is given in Table VII.

To determine the production of $\Sigma^+(1385)$ via

$$\gamma p \to \Sigma^+(1385)K^0, \qquad (12')$$

only events of reaction (12) with a *visible* K^0 *decay* have been plotted, whether the Λ decay was seen or not. The corresponding distribution of the $\Lambda\pi^+$ effective mass (not shown) has a peak in the $\Sigma^+(1385)$ mass region. Events with additional neutral pions, according to $\gamma p \to \Lambda K^0\pi^+\pi^0(\pi^0\cdots)$, may contribute to this $\Lambda\pi^+$ mass

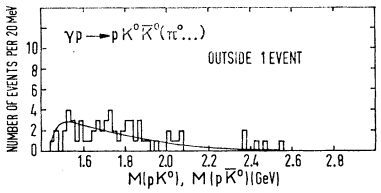

FIG. 34. Reaction $\gamma p \to pK^0\bar{K}^0(\pi^0\cdots)$ for $E_\gamma<5.8$ GeV. Distribution of the pK^0, $p\bar{K}^0$ effective masses $M(pK^0)$, $M(p\bar{K}^0)$. The curve shows Lorentz-invariant phase space.

distribution; however, due to its small width the $\Sigma^+(1385)$ peak can come only from events without π^0 i.e., it comes from reaction (12′). The cross section for (12′) which is corrected for events with invisible K^0 decay and unobserved decay modes, is given in Table VII.

Evidence for $\Sigma^+(1385)$ production via

$$\gamma p \to \Sigma^+(1385) K^0 \pi^0 (\pi^0 \cdots) \qquad (12'')$$

comes from the $\Lambda\pi^+$ effective-mass distribution in Fig. 32, which contains *all* events of reaction (12). In this distribution the peak in the $\Sigma^+(1385)$ mass region cannot be completely explained by the cross section found for reaction (12′). As Fig. 32 contains also events from reaction $\gamma p \to \Lambda K^0 \pi^+ \pi^0 (\pi^0 \cdots)$, we conclude that a part of the $\Sigma^+(1385)$ peak in Fig. 32 is due to $\Sigma^+(1385)$ production via (12″).

Strong production of the $\Sigma(1385)$ resonance via $\gamma p \to \Sigma(1385) K \to (\Lambda\pi) K$ has also been observed by the Cambridge Bubble-Chamber Group.[6]

In Fig. 32, an enhancement of 23 ± 7 events at about 1765 MeV is seen in the $\Lambda\pi^+$ mass distribution of reaction (12). If this peak is due to the production of $\Sigma^+(1765)$ via $\gamma p \to \Sigma^+(1765) K^0$, one expects from the branching ratio[20] of $\Sigma^+(1765)$ a bump of 30–40 events above background in the $p\bar{K}^0$ mass distribution at the same mass value. However, in the experimental pK^0, $p\bar{K}^0$ mass distribution of reaction $\gamma p \to p K^0 \bar{K}^0 (\pi^0 \cdots)$ (Fig. 34), only 12 events are seen in the mass region 1720–1820 MeV.

The accumulation of events above the phase-space curve in Fig. 32 at low ΛK^0 effective masses cannot be primarily due to an N^* with mass of about 1680 MeV, since then the reaction $\gamma p \to N^*(1680)\pi^+ \to (p\pi^-)\pi^+$ would have been clearly observed (see Ref. 1). In reactions (11)–(15), no significant $K^*(890)$ production is found. This is consistent with the small values of the $K^*K\gamma$ partial decay widths $\Gamma(K^{*\pm}K^\pm\gamma) = 0.075$ MeV and $\Gamma(K^{*0}K^0\gamma) = 0.125$ MeV,[30] as predicted by SU_6.

Apart from the $\Sigma(1385)$, no significant production of other resonances in reactions (11)–(15) is observed in this experiment.

ACKNOWLEDGMENTS

We are pleased to express our appreciation to the staff of DESY for making available to us the facilities of the synchrotron, the bubble chamber, and the photon beam; and to our scanning and computing groups for their efforts in the analysis of the data. We also thank Dr. K. Böckmann and Dr. P. Söding for valuable discussions. The work in Aachen, Bonn, Hamburg, Heidelberg, and München was supported by the Bundesministerium für Wissenschaftliche Forschung.

[30] F. C. Chan, Nuovo Cimento **45**, 259 (1966).

APPENDIX: FITTING PROCEDURE FOR THE REACTION $\gamma p \to p\pi^+\pi^-\pi^0$

The contributions of the different resonance- and background-production processes to the reaction $\gamma p \to p\pi^+\pi^-\pi^0$, which are listed in Table II, were obtained by fitting the following density distribution to the data, using the maximum-likelihood method:

$$\frac{d^6N}{dM_{-0}^2 dM_{p+}^2 dM_{+-}^2 dM_{+-0}^2 dM_{p+-}^2 dE_\gamma} = \left(a_0 \frac{BW_0}{N_0} + a_1 \frac{BW_1}{N_1} + \cdots + a_m \frac{BW_m}{N_m}\right) \frac{H(E_\gamma)}{E_{\text{c.m.}}^2 \sqrt{B}}, \qquad \text{(A1)}$$

where $+$, 0, and $-$ stand for π^+, π^0, and π^-, respectively. The five effective masses M_{-0}, M_{p+}, M_{+-}, M_{+-0}, M_{p+-} are independent variables describing the final state; all the other effective masses can be expressed by them. a_k is the number of events belonging to process k; $a_0 + a_1 + \cdots + a_m$ is the total number of events in the E_γ interval considered. The numbers $a_1, \cdots, a_m$ are to be determined by the fit. $BW_0 = 1$ describes the Lorentz-invariant phase-space background. BW_k ($k = 1, \cdots, m$) is a Breit-Wigner term describing the resonance production in process k.[31] If only one resonance decaying into two particles is produced, then

$$BW_k(M) = \frac{M}{q} \frac{M_0\Gamma}{(M_0^2 - M^2)^2 + M_0^2\Gamma^2}, \qquad \text{(A2)}$$

where $q(M)$ is the modulus of the 3-momentum of the decay particles in the resonance rest system; $\Gamma(M)$ is the mass-dependent width $= \Gamma_0 [q(M)/q(M_0)]^3 \rho(M)/\rho(M_0)$; $\rho(M) = [2.2 m_\pi^2 + q(M)^2]^{-1}$ for the Δ resonance; $\rho(M) = [q(M_0)^2 + q(M)^2]^{-1}$ for the ρ resonance; M_0 and Γ_0 are mass and width of the resonance; and m_π is the mass of the pion.

If process k contains simultaneous production of two resonances (e.g., $\gamma p \to \Delta^{++}\rho^-$), then BW_k is the product of two terms of the form (A2), each of them describing one of the resonances. For the ω contribution, we used a Gaussian distribution

$$BW_\omega(M) = \exp[-(M - M_0)^2/2\sigma^2].$$

N_k is a normalization factor given by

$$N_k = \int BW_k \frac{H(E_\gamma)}{E_{\text{c.m.}}^2 \sqrt{B}} \times dM_{-0}^2 dM_{p+}^2 dM_{+-}^2 dM_{+-0}^2 dM_{p+-}^2 dE_\gamma. \qquad \text{(A3)}$$

$E_{\text{c.m.}}$ is the total energy in the c.m. system. $H(E_\gamma)$ describes the photon-energy dependence of the density distribution.

When multiplying each Breit-Wigner term BW_k with the same factor $H(E_\gamma)$, one assumes that within the

[31] J. D. Jackson, Nuovo Cimento **34**, 1644 (1964).

E_γ interval over which the fit is carried out, the cross sections $\sigma_k(E_\gamma)$ for all processes k are proportional to one another. This assumption is certainly justified when the E_γ interval is small. $H(E_\gamma)$ is determined from the experiment by the requirement that $H(E_\gamma)R_4(E_\gamma)$ describes the observed photon-energy distribution of all events belonging to reaction $\gamma p \to p\pi^+\pi^-\pi^0$, where

$$R_4(E_\gamma)=\int \frac{1}{E_{\text{c.m.}}{}^2\sqrt{B}} dM_{-0}{}^2 dM_{p+}{}^2 dM_{+-}{}^2 dM_{+-0}{}^2 dM_{p+-}{}^2$$

is the four-particle phase space. B is a function of all independent effective masses, defined by Eq. (7) of Ref. 32.

Of the six integrations appearing in (A3), three can be performed analytically[32] while the other three integrations are done numerically.

Using the density distribution (A1) one neglects possible interference terms between the amplitudes for resonance and background production.

[32] P. Nyborg *et al.*, Phys. Rev. **140**, B914 (1965).

PHYSICAL REVIEW VOLUME 188, NUMBER 5 25 DECEMBER 1969

Asymmetry Parameter and Branching Ratio of $\Sigma^+ \to p\gamma$*

LAWRENCE K. GERSHWIN,† MARGARET ALSTON-GARNJOST, ROGER O. BANGERTER, ANGELA BARBARO-GALTIERI, TERRY S. MAST, FRANK T. SOLMITZ, AND ROBERT D. TRIPP

Lawrence Radiation Laboratory, University of California, Berkeley, California 94720

(Received 25 August 1969)

An experiment to study the decay $\Sigma^+ \to p\gamma$ was performed in the Berkeley 25-in. hydrogen bubble chamber. An analysis was made of 48 000 events of the type $K^-p \to \Sigma^+\pi^-$, $\Sigma^+ \to p$+neutral with K^- momenta near 400 MeV/c. The Σ's produced in this momentum region are polarized because of the interference of the Y_0^* (1520) amplitude with the background amplitudes. We have measured the proton asymmetry parameter α for 61 $\Sigma^+ \to p\gamma$ events with an average polarization of 0.4. We found $\alpha = -1.03_{-0.42}{}^{+0.52}$. $SU(3)$ predicts a value $\alpha = 0$. A more restricted sample of events was used to determine the $\Sigma^+ \to p\gamma$ branching ratio. From 31 $\Sigma^+ \to p\gamma$ events and 11 670 $\Sigma^+ \to p\pi^0$ events, we found $(\Sigma^+ \to p\gamma)/(\Sigma^+ \to p\pi^0) = (2.76 \pm 0.51) \times 10^{-3}$. The result is in agreement with the previous measurements.

I. EXPERIMENTAL PROCEDURE

AN exposure of 1.3×10^6 pictures in the Berkeley 25-in. hydrogen bubble chamber yielded about 57 000 events of the type $K^-p \to \Sigma^+\pi^-$, $\Sigma^+ \to p$ +neutral, with K^- momenta ranging from 270 to 470 MeV/c. The vast majority of the events were near 390 MeV/c, where the $Y_0^*(1520)$ resonance is formed. Of the 48 000 measured events, we were able to identify 61 events of the decay $\Sigma^+ \to p\gamma$.

The problem in the experiment was to separate the rare $\Sigma^+ \to p\gamma$ decays from the more copious $\Sigma^+ \to p\pi^0$ decays.[1] The proton momentum in the rest frame of the Σ is 189.0 MeV/c for $\Sigma^+ \to p\pi^0$ and 224.6 MeV/c for $\Sigma^+ \to p\gamma$. Bazin *et al.*[2] found a branching ratio of $(3.7 \pm 0.8) \times 10^{-3}$, using only events with stopped protons. For such events the proton momentum is determined from range rather than curvature, and is thus very accurately known, so that the two decay modes are almost always distinguishable.

Some events with protons which left the chamber were also used in this experiment. Generally such events present considerable resolution difficulty because the proton momentum is determined from the curvature measurement, and the associated error in the momentum is determined by the large multiple Coulomb scattering. The $\Sigma^+ \to p\gamma$ decay, however, releases more momentum to the proton than does the $\Sigma^+ \to p\pi^0$ decay, so that it is sometimes possible for the lab-system angle between the proton and the Σ in a $\Sigma^+ \to p\gamma$ decay to exceed the maximum possible angle for a $\Sigma^+ \to p\pi^0$ decay, for a given Σ momentum. Since the angles were well measured, many $\Sigma^+ \to p\gamma$ decays could be identified because of an excessive lab decay angle. A smaller contribution to the $\Sigma^+ \to p\gamma$ sample came from events with a leaving or scattering proton in which the proton-track length was too great for the proton to be from a $\Sigma^+ \to p\pi^0$ decay.

II. ASYMMETRY PARAMETER

The scanners were required to distinguish between $\Sigma^+ \to p$ decays and $\Sigma^+ \to \pi^+$ decays by ionization. Those events identified as $\Sigma^+ \to p$ decays were fitted to the hypotheses

(i) $K^-p \to \Sigma^+\pi^-$, $\Sigma^+ \to p\pi^0$,

(ii) $K^-p \to \Sigma^+\pi^-$, $\Sigma^+ \to p\gamma$,

* Work done under the auspices of the U. S. Atomic Energy Commission.

† Present address: Nevis Laboratories, Columbia University, Irvington, N. Y.

[1] A more detailed discussion of the experiment can be found in L. K. Gershwin (Ph.D. thesis), University of California Lawrence Radiation Laboratory Report No. UCRL-19246, 1969 (unpublished).

[2] M. Bazin, H. Blumenfeld, U. Nauenberg, L. Seidlitz, and C. Y. Chang, Phys. Rev. Letters **14**, 154 (1965).